NANOCELLULOSE-CHITOSAN-METAL ORGANIC

FRAMEWORK COMPOSITES FOR ARSENIC REMOVAL

Miss Yatika Paisart

จุฬาลงกรณ์มหาวิทยาลัย

CHULALONGKORN UNIVERSITY

A Thesis Submitted in Partial Fulfillment of the Requirements

for the Degree of Master of Science in Chemistry

Department of Chemistry

FACULTY OF SCIENCE

Chulalongkorn University

Academic Year 2021

นาโนเซลลูโลส-ไคโตซาน-โครงข่ายโลหะอินทรีย์คอมพอสิตสำหรับการขจัดอาร์ซีนิก

น.ส.ญาติกา ไพสาทย์

วิทยานิพนธ์นี้เป็นส่วนหนึ่งของการศึกษาตามหลักสูตรปริญญาวิทยาศาสตรมหาบัณฑิต
สาขาวิชาเคมี ภาควิชาเคมี
คณะวิทยาศาสตร์ จุฬาลงกรณ์มหาวิทยาลัย
ปีการศึกษา 2564

Thesis Title	NANOCELLULOSE-CHITOSAN-METAL ORGANIC FRAMEWORK COMPOSITES FOR ARSENIC REMOVAL
By	Miss Yatika Paisart
Field of Study	Chemistry
Thesis Advisor	Associate Professor FUANGFA UNOB, Ph.D.

Accepted by the FACULTY OF SCIENCE, Chulalongkorn University in Partial Fulfillment of the Requirement for the Master of Science

.... Dean of the FACULTY OF SCIENCE

(Professor POLKIT SANGVANICH, Ph.D.)

THESIS COMMITTEE

.... Chairman

(Professor VUDHICHAI PARASUK, Ph.D.)

.... Thesis Advisor

(Associate Professor FUANGFA UNOB, Ph.D.)

.... Examiner

(Assistant Professor WIPARK ANUTRASAKDA, Ph.D.)

.... External Examiner

(Associate Professor Panya Sunintaboon, Ph.D.)

ญาติกา ไพสาทย์ : นาโนเซลลูโลส-ไคโตซาน-โครงข่ายโลหะอินทรีย์คอมพอสิตสำหรับการขจัด
อาร์ซีนิก. (NANOCELLULOSE-CHITOSAN-METAL ORGANIC
FRAMEWORK COMPOSITES FOR ARSENIC REMOVAL) อ.ที่ปรึกษาหลัก : รศ. ดร.
เฟื่องฟ้า อุ่นอบ

ในงานนี้ ทำการสังเคราะห์ฟองน้ำคอมพอสิตแบบใหม่จากไคโตซาน นาโนเซลลูโลส และ
โครงข่ายโลหะอินทรีย์ MIL-53(Fe) สำหรับใช้ในการกำจัดอาร์ซีไนต์และอาร์ซีเนต โดยทำการเตรียมนาโน
เซลลูโลสที่มีขนาดเฉลี่ย 433.5 ± 41.0 นาโนเมตรและสังเคราะห์ผลึกทรงแปดด้านของ MIL-53(Fe) นำ
นาโนเซลลูโลสที่เตรียมได้ผสมเข้ากับไคโตซานและ MIL-53(Fe) ก่อนทำการเชื่อมขวางและทำให้แห้งด้วย
การแช่เยือกแข็ง จากนั้นนำวัสดุที่ได้ไปพิสูจน์เอกลักษณ์ด้วยเทคนิคฟูเรียร์ทรานส์ฟอร์มอินฟราเรดสเปก
โทรสโกปี การดูดซับไนโตรเจน กล้องจุลทรรศน์อิเล็กตรอนแบบส่องกราด และเทคนิคการวิเคราะห์ธาตุ
และองค์ประกอบ ผลการวิจัยพบว่าสามารถสังเคราะห์ฟองน้ำคอมพอสิตได้สำเร็จด้วยอัตราส่วนน้ำหนักที่
เหมาะสมคือ 2CS: 1NC: 1.5MIL-53(Fe) โดยคอมพอสิต CS-NC-MIL-53(Fe) มีโครงสร้างที่มีรูพรุนสูง
และมีพื้นที่ผิว 8.70 ตารางเมตร/กรัม หลังจากนั้นได้ทำการศึกษาสภาวะที่เหมาะสมในการกำจัดอาร์ซีนิก
ในสารละลายด้วยวัสดุคอมพอสิตที่เตรียมได้ ปัจจัยที่ทำการศึกษาได้แก่ ค่าความเป็นกรดเบสของ
สารละลายอาร์ซีนิก ระยะเวลาในการกำจัดอาร์ซีนิก ความเข้มข้นเริ่มต้นของสารละลายอาร์ซีนิก และ
ไอออนที่รบกวน โดยคอมพอสิตนี้สามารถกำจัดอาร์ซีไนต์และอาร์ซีเนตออกจากสารละลายได้ในช่วงค่า
ความเป็นกรดเบสเท่ากับ 9-11 และ 3-11 ตามลำดับ เวลาที่เหมาะสมสำหรับการกำจัดคือ 6 ชั่วโมง
จลนพลศาสตร์ของการดูดซับอาร์ซีไนต์และอาร์ซีเนตเป็นไปตามแบบจำลองจลนพลศาสตร์อันดับสอง
เทียม และไอโซเทอร์มการดูดซับเป็นไปตามแบบจำลองแลงเมียร์ไอโซเทอร์ม คอมพอสิตมีความจุการดูด
ซับสูงสุดสำหรับอาร์ซีไนต์คือ 8.53 มก./กรัม และอาร์ซีเนตคือ 36.76 มก./กรัม ไอออนที่ส่งผลรบกวนที่
อาจพบ ได้แก่ ฟอสเฟตและซัลเฟตไอออน นอกจากนี้ คอมพอสิตยังมีสมบัติทางกลที่ดีและมีความเสถียร
ในน้ำ โดยได้ประยุกต์ใช้คอมพอสิตนี้ในการกำจัดอาร์ซีนิกในตัวอย่างน้ำเสียจากอุตสาหกรรมการกลั่น
ปิโตรเลียม

สาขาวิชา	เคมี	ลายมือชื่อนิสิต ....
ปีการศึกษา	2564	ลายมือชื่อ อ.ที่ปรึกษาหลัก ....

6172126023 : MAJOR CHEMISTRY

KEYWORD: Chitosan, Nanocellulose, Composite, Metal-organic framework MIL-53(Fe), Arsenic removal

Yatika Paisart : NANOCELLULOSE-CHITOSAN-METAL ORGANIC FRAMEWORK COMPOSITES FOR ARSENIC REMOVAL. Advisor: Assoc. Prof. FUANGFA UNOB, Ph.D.

In this work, a new composite sponge of chitosan, nanocellulose, and MIL-53(Fe) metal-organic-framework were synthesized and applied for As(III) and As(V) removal. Nanocellulose with an average size of 433.5 ± 41.0 nm were prepared and used. The octahedron crystalline MIL-53(Fe) was successfully synthesized. The nanocellulose was mixed with chitosan and MIL-53(Fe) before crosslinking and freeze-drying. The obtained materials were characterized by Fourier transform infrared spectroscopy, nitrogen adsorption, scanning electron microscope, and energy dispersive x-ray spectroscopy. The results showed that the composite sponge was successfully fabricated with a suitable weight ratio of 2CS: 1NC: 1.5MIL-53(Fe). The CS-NC-MIL-53(Fe) composite exhibited a highly porous structure with the surface area of 8.70 m^2/g. The composite was further used to adsorb As(III) and As(V) in solutions. The effect of the solution pH, contact time, initial concentration of arsenic, and interfering ions were investigated. The composite could remove As(III) and As(V) from solutions in the pH range of 9-11 and 3-11, respectively. The suitable contact time for arsenic removal was 6 h. The kinetics of As(III) and As(V) adsorption followed pseudo-second order and the adsorption isotherm fit well to the Langmuir model. The maximum adsorption capacities were 8.53 mg/g and 36.76 mg/g for As(III) and As(V), respectively. The potential interfering ions included phosphate and sulfate ions. Furthermore, the composite showed good mechanical property and stability in water. Their application to remove arsenic in wastewater samples from a petroleum refining industry was demonstrated.

Field of Study: Chemistry   Student's Signature ....

Academic Year: 2021   Advisor's Signature ....

ACKNOWLEDGEMENTS

จุฬาลงกรณ์มหาวิทยาลัย
CHULALONGKORN UNIVERSITY

TABLE OF CONTENTS

Page

LIST OF TABLES

LIST OF FIGURES

CHAPTER 1

INTRODUCTION

1.1 Statement of the problem

Economic progress and industrial expansion have all contributed to heavy metal contamination in the environment in recent decades, particularly hazardous metals like arsenic. Arsenic contamination in water sources has aroused global concerns due to its high toxicity and danger to the ecosystems in the long term [1-3].

Arsenic (As) is known as metalloid element that is strongly carcinogenic to human, and commonly found in natural water and industrial wastewater. Arsenic exists in both organic and inorganic forms and the inorganic arsenic is more poisonous than the organic species. The most prevailing types of inorganic arsenic in aqueous system are As(III) known as arsenite and As(V) also known as arsenate which displays in oxyanions forms [4, 5].

Mostly, the source of arsenic contamination in the environment comes from human activities such as mining, metallurgy, tanning, petroleum refining, and other manufacturing [6, 7]. The level of arsenic in the effluent from these processes should be controlled to prevent the contamination in the environmental resources. The World Health Organization (WHO) and the U.S. Environmental Protection Agency (USEPA) limit the level of arsenic in drinking water to 10 µg/L [8]. For industrial effluent, the Pollution Control Department of Thailand (PCD) states that the arsenic concentration should not exceed 0.25 mg/L [9].

Several water treatment approaches are used for arsenic removal including oxidation, co-precipitation, ion-exchange, membrane technologies, electrochemical, and adsorption [8, 10, 11]. Adsorption is one of the most popular used techniques for eliminating arsenic from water due to its easy operation and effectiveness. Many

types of sorbents have been studied for arsenic adsorption such as activated carbon, alumina, metal oxides, and natural sorbents [12-16]. Recently, biopolymers such as chitosan has gained much attention from researchers for the application in many fields including as adsorbents for arsenic removal [17-19].

Chitosan (CS) is a low cost and plentiful biopolymer that has unique structure bearing amine (-NH$_2$) groups, suitable for heavy metals adsorption [20-22]. Moreover, to improve its adsorption efficiency, chitosan has been fabricated in a sponge form with interesting properties including a higher porosity, a larger specific surface area, and better adsorption, compared to its original form [23]. However, the application of chitosan sponge is limited by its low stability in aqueous phase and poor mechanical property. To overcome these shortcomings, the chitosan sorbents reinforced with various modifier/fillers (e.g. cellulose) have been developed to suit its practical applications [24-28].

In this work, a chitosan sponge reinforced with nanocellulose was fabricated and applied for arsenic removal. The nanocellulose was chosen as the reinforcement filler due to its high mechanical strength and eco-friendly. Additionally, to enhance the efficiency in arsenic removal, chitosan-nanocellulose (CS-NC) composite was modified with a metal-organic frameworks (MOFs), MIL-53(Fe). In general, MOFs have been demonstrated to have good adsorption capacity for heavy metal with interesting properties such as high specific surface area and adjustable functionality [29, 30]. The MIL-53(Fe) is a class of MOFs that contains Fe(III) ions as metal centers that is low toxic and has affinity towards arsenic coordination. Furthermore, it is stable in water and easy to synthesize [31, 32].

1.2 Objectives of the thesis

The objectives of this work are to synthesize the chitosan-nanocellulose (CS-NC) composite sponge modified with the metal-organic framework MIL-53(Fe) and use in arsenite and arsenate adsorption.

1.3 Scope of the thesis

At the beginning of this work, the nanocellulose (NC) was synthesized from crystalline microcellulose and characterized by dynamic light scattering (DLS), transmission electron microscope (TEM), and Fourier transform infrared spectroscopy (FT-IR). The metal-organic framework MIL-53(Fe) was synthesized by solvothermal method and characterized by X-ray diffraction spectroscopy (XRD), Fourier transform infrared spectroscopy (FT-IR), N_2 adsorption, and scanning electron microscopy (SEM). After that, the nanocellulose and MIL-53(Fe) were used to prepare CS-NC-MIL-53(Fe) composites sponge by freeze-drying method. The parameters affecting the CS-NC-MIL-53(Fe) preparation were investigated and optimized. The final CS-NC-MIL-53(Fe) composites sponge was characterized for its surface area and morphology by N_2 adsorption, and scanning electron microscopy, respectively.

For the adsorption study, factors affecting the As(III) and As(V) removal by CS-NC-MIL-53(Fe) adsorbent such as initial pH of arsenic solution, contact time, initial concentration, and interfering ions were investigated to find the optimum conditions. Finally, the composite material was used to adsorb arsenic in real water samples. The concentrations of the arsenic in solutions were determined by inductively coupled plasma - optical emission spectrometer (ICP-OES).

1.4 The benefits of this thesis

To obtain a chitosan-nanocellulose composite sorbent that has a potential for arsenic removal from water.

CHAPTER 2
THEORY AND LITERATURE REVIEW

2.1 Arsenic

Arsenic (As) is a metalloid element of the earth's crust, widely distributed in the environment including air, water, and land. It is a highly toxic chemical that leads to severe consequences on human and animal health. Arsenic can be released to water resources from both the natural causes and human activities. For the natural processes, arsenic is released from the rocks and volcanic rocks through weathering and microbial activities. On the other hand, human activities such as mining, metallurgy, tanning, petroleum refining, and other manufacturing processes are dominant routes to cause arsenic contamination in the environment which is a global concern [4-7].

2.1.1 Chemical properties of arsenic in water

In the aqueous environment, arsenic mostly exists in two oxidation states, +3 and +5 which appear as soluble oxyanion arsenic in inorganic forms. Inorganic arsenic, arsenite (+3) and arsenate (+5) are more commonly found in water, hereinafter referred to as As(III) and As(V), respectively. As(III) is the predominant form under reducing conditions, whereas As(V) is the dominant stable form in oxygenated water. The species of As(III) and As(V) can be in their protonated/deprotonated forms depending on the redox potential and pH of an aqueous environment. The dissociation and pK_a values are present in Figure 2.1. The distribution of As(III) and As(V) species at different solution pH are shown in Figure 2.2. For As(V), it is solely in the form of H_3AsO_4 and AsO_4^{3-} at pH < 2 and > 12, respectively. Meanwhile, the forms of $H_2AsO_4^-$, $HAsO_4^{2-}$, and their mixtures are found in the pH range of 3-11. For

As(III), most form is uncharged species like H_3AsO_3, while the negatively charged species of As(III) ($H_2AsO_3^-$, $HAsO_3^{2-}$, AsO_3^{3-}) are present at pH higher than 8 [4, 8, 33].

$$H_3AsO_4 \xrightarrow[\text{pKa}=2.1]{-H^+} H_2AsO_4^- \xrightarrow[\text{pKa}=6.7]{-H^+} HAsO_4^{2-} \xrightarrow[\text{pKa}=11.2]{-H^+} AsO_4^{3-}$$

$$H_3AsO_3 \xrightarrow[\text{pKa}=9.1]{-H^+} H_2AsO_3^- \xrightarrow[\text{pKa}=12.1]{-H^+} HAsO_3^{2-} \xrightarrow[\text{pKa}=13.4]{-H^+} AsO_3^{3-}$$
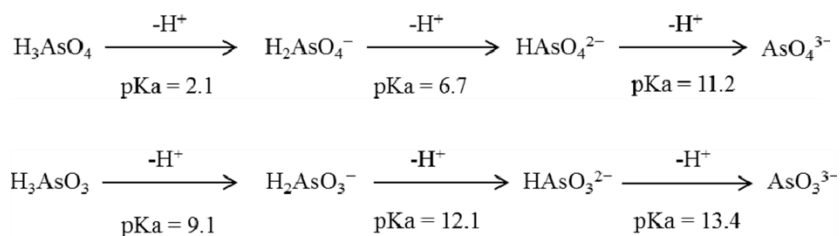
Figure 2.1 Dissociation reaction of As(V) and As(III) species.
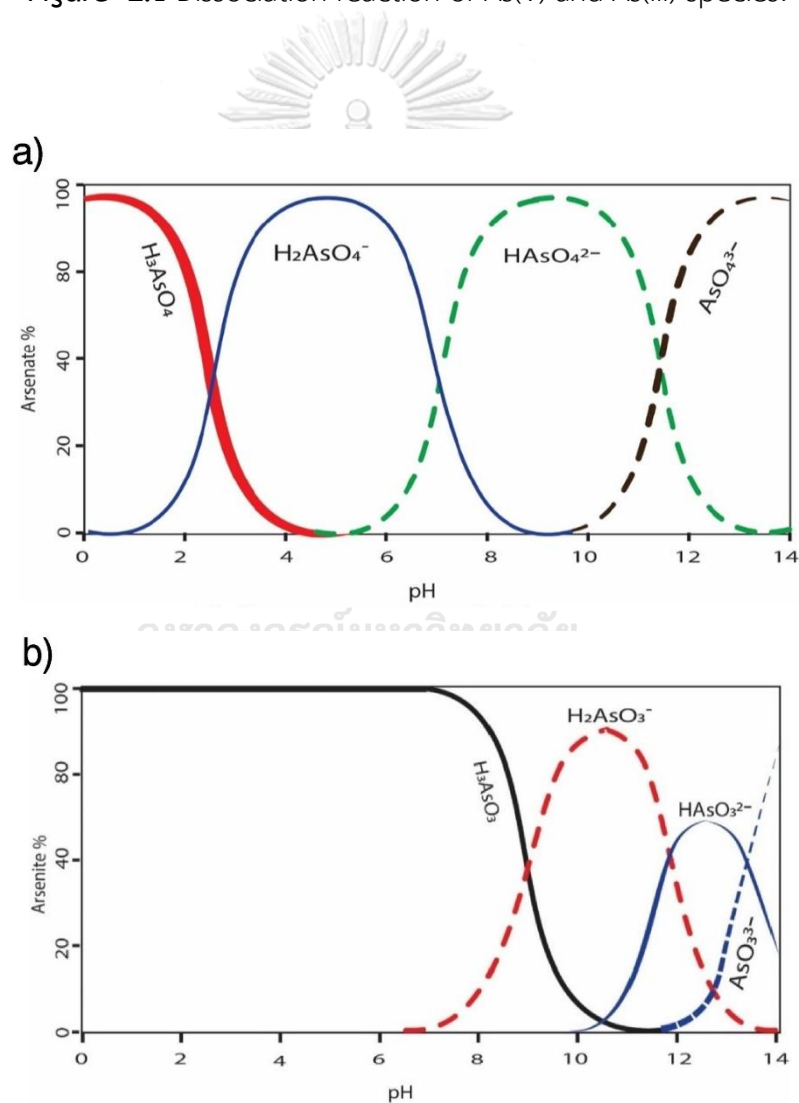
Figure 2.2 The distribution of (a) As (V) and (b) As(III) species
at different pH values [8].

2.1.2 Toxicity of arsenic

Arsenic is a toxic element that causes adverse effect on human and animal health. Contamination of arsenic in water resource caused by industrial activity is one of the most common routes. Although a small intake of arsenic helps to maintain the immune system activity in human, an exposure to high dose arsenic is fatal. Moreover, inorganic arsenic is more toxic than the organic species and As(III) and As(V) are both human carcinogens, according to the International Agency for Research on Cancer (IARC). It may cause skin, liver, lungs, kidney, and urinary bladder cancers. Furthermore, long-term consumption of arsenic-contaminated water causes cardiovascular and gastrointestinal diseases, skin pigmentation, central nervous system damage, lack of appetite, diabetes, muscle weakness, etc. [4, 7, 33]. To prevent the arsenic contamination, controlling arsenic level in industrial effluent is mandatory. Therefore, both the World Health Organization (WHO) and the United States Environmental Protection Agency (USEPA) set the limit of arsenic level in drinking water to 10 µg/L [8]. For industrial wastewater, the Pollution Control Department of Thailand (PCD) has set a maximum allowed level of arsenic to 0.25 mg/L [9]. The methods for removing arsenic from contaminated water are described in the next section.

2.1.3 Technologies for arsenic removal

To remove arsenic from contaminated water, several water treatment techniques have been applied such as oxidation, co-precipitation, ion-exchange, membrane technologies, electrochemical, and adsorption. Adsorption is one of the most popular techniques used due to its several advantages including use of less additional chemicals, ease of operation, and effectiveness [8, 10, 11].

2.2 Adsorbent

An adsorbent is a solid substance used to remove contaminants from liquid or gas through different interactions on the surface of solid material. The adsorbents are particularly significant in the adsorption process because they affect the removal efficiency. The material physical and chemical properties such as mechanical strength, porosity, surface area, and chemical functional groups determine the efficiency of the adsorbent in the adsorption process. Many types of adsorbents have been studied for arsenic removal including activated carbon, alumina, metal oxides, and natural materials [5, 12-16].

Nowadays, bio-based sorbents have gained much attention for water treatment and arsenic removal due to their low cost, cost-effectiveness, and non-toxicity [8, 33, 34]. In this work, a composite derived from biomasses (i.e. chitosan and cellulose) was fabricated for removing arsenic. Its performance was further enhanced by adding a metal organic framework.

2.2.1 Chitosan

Chitosan (CS) is a biopolymer derived from waste seafood shells. It is low cost, non-toxic, biodegradable, biocompatible, and eco-friendly. it has been applied in many fields including medical and environmental applications. Chitosan is a hydrophilic material bearing hydroxyl (-OH) and amine (-NH$_2$) functional groups on the polymer chains as shown in Figure 2.3. These functional groups act as active sites for the modification and serve for coordination and electrostatic interaction with targeted metal ions. For example, under acidic condition, the protonated amine groups of chitosan have shown good affinity toward anions including anionic arsenic species [17-22, 33]. However, chitosan can be dissolved in aqueous media under acidic or basic conditions, limiting its application. Hence, many researches have been carried out to improve the physical and mechanical properties of chitosan.
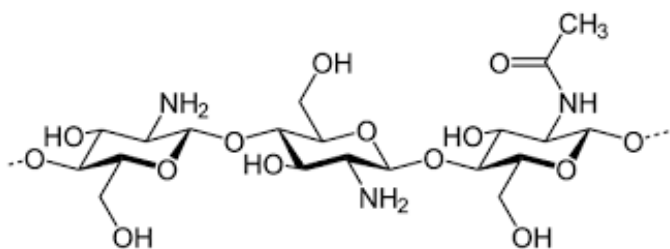
Figure 2.3 The structure of chitosan [35].

2.2.2 Modification of chitosan for arsenic removal

For the application of chitosan for water treatment, different approaches for chitosan modification have been done to improve its mechanical strength, stability in water, and the adsorption capacity (Figure 2.4). Chitosan can be modified by blending/compositing, crosslinking, and grafting with other polymers or chemicals to improve its mechanical strength and stability. The chitosan blending can be done by mixing chitosan with other polymers or chemicals under suitable conditions. For the adsorption purpose, a variety of modifier/fillers were used in the blending with chitosan including magnetite, zero-valent iron, cellulose, etc. Meanwhile, the crosslink technique can be performed using chemicals like glutaraldehyde as crosslinking agent. However, the crosslinking with aldehyde reduces the number of free amino groups for adsorption. For the grafting technique, a chemical initiator or radiation-induced procedure is required to start the grafting process. Furthermore, various parameters such as grafting route and reaction temperature have to be controlled [33, 36, 37].
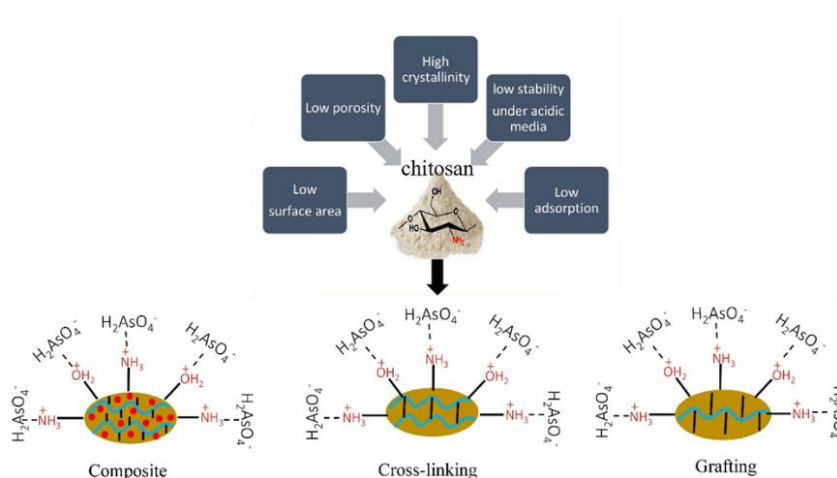
Figure 2.4 Modification of chitosan for removal of arsenate [8].

Alternatively, the physical properties of chitosan can be improved by physical alterations. Typically, commercial chitosan is in flakes or powder form that possesses low surface area and low porosity. The usage of the chitosan of these forms without modification may encounter clog or difficulty in solid separation from aqueous solution. Hence, chitosan has been used in different forms to overcome the problem and one of alternatives is to fabricate chitosan in sponge form. Chitosan in sponge structure can be obtained by freeze-drying method. It possesses a higher porosity, larger specific surface area, and good water uptake, showing high potential for adsorption application. With this porous structure, it increases arsenic mobility in the adsorbent, boosting the adsorption rate [23-28, 33]. Nevertheless, pure chitosan sponge has poor mechanical property and water stability when used as adsorbent in aqueous solution. Thus, to improve the mechanical properties and water stability of the chitosan sponge, it should be combined with other polymers or chemicals through blending/compositing, crosslinking, and grafting methods [8].

The blending technique and sponge fabrication were chosen in this work to produce chitosan adsorbent due to their simple operation. Nanocellulose and metal-organic frameworks (MOFs) were blended with chitosan prior to sponge formation to

enhance its mechanical strength and the adsorption capacity. The unique properties of these fillers are described in the next section.

Cellulose/nanocellulose

Cellulose is a low cost and eco-friendly material that can be extracted from different bio-sources. Nanocellulose is typically produced from cellulose by acid hydrolysis, enzymatic hydrolysis, and mechanical process. The properties of nanocellulose include low density, large surface area, and high strength. Thus, cellulose and nanocellulose are often used to reinforce chitosan material to improve the mechanical strength. Furthermore, cellulose/nanocellulose contains hydroxyl (-OH) groups in their structure (Figure 2.5) that can form hydrogen bonding with amine groups in chitosan [25-27]. This interaction would result in a homogenous distribution of nanocellulose in chitosan matrix.
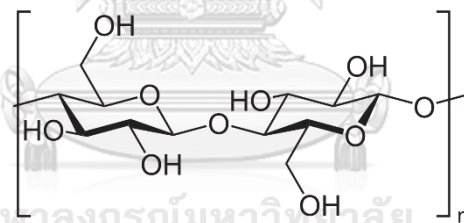
Figure 2.5 The structure of cellulose.

Metal-organic framework

Metal-organic frameworks (MOFs) are crystalline porous materials synthesized through the coordination of metal ions/clusters with organic ligands to create framework as simply shown in Figure 2.6. MOFs have received a lot of attention in many fields including adsorption due to its good adsorption capacity for heavy metal, high specific surface area, and adjustable functionality [29, 30]. The Material Institute of Lavoisier (MIL) MOF, MIL-53(Fe), were used to produce a composite in this work to

enhance the adsorption capacity toward arsenic species. The high-valent irons (Fe^{3+}) and terephthalic acid were used as metal ion center and organic ligand, respectively. The MIL-53(Fe) has a good chemical resistance, water stability, and it is easy to synthesize [31, 32, 38]. More importantly, it is a low toxic material as the metal centers of MIL-53 are iron [32]. Typically, MIL-53(Fe) framework was synthesized by solvothermal process as shown in Figure 2.7 [39]. The chemical structure of MIL-53(Fe) is presented in Figure 2.8 [40].
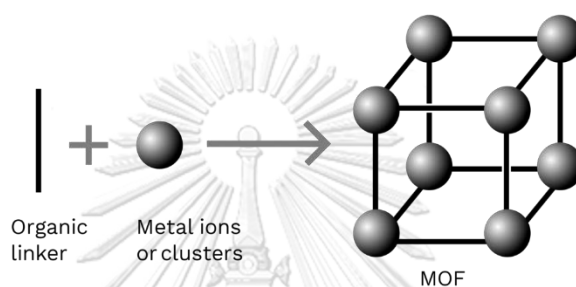
Figure 2.6 Synthesis concept of metal-organic framework (MOF).
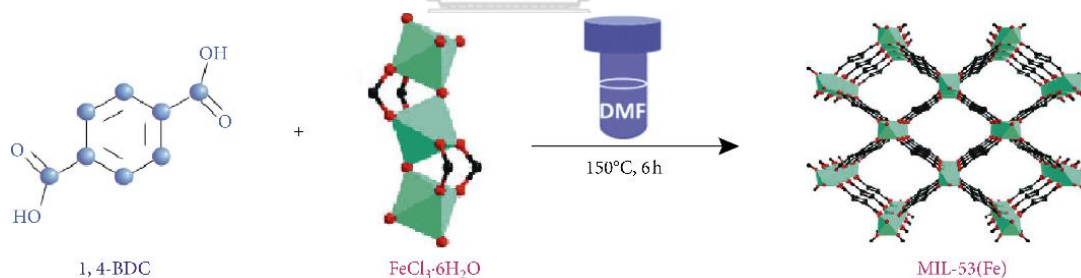
Figure 2.7 Synthesis of MIL-53(Fe) framework [39].
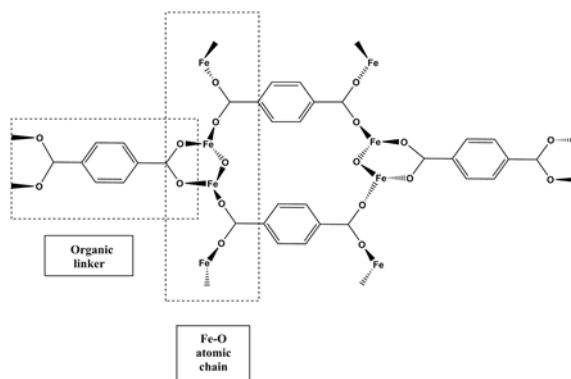
Figure 2.8 The chemical structure of MIL-53(Fe) [40].

2.3 Adsorption

Adsorption is a process that involves the accumulation of analytes (in liquid or gas phase) on the surface of an insoluble solid material which is called mass transfer process. The analyte that deposits on the surface is referred to an adsorbate, whereas the solid material as an adsorbent. According to the interaction types and forces between adsorbate and adsorbent, adsorption process can be divided into two types including physisorption and chemisorption [41-43].

Physisorption (physical adsorption)

Physisorption is the physical interaction between the molecules of adsorbate and the surface of adsorbents via Van der Waals force attraction or electrostatic interaction. This interaction between the adsorbent surface and adsorbate is non-specific and the adsorption may occur as multiple layers adsorption on the surface. It has low adsorption heat and has low binding energy between adsorbent and adsorbate.

Chemisorption (chemical adsorption)

Chemisorption of the adsorbate occurs through the formation of chemical bond between the adsorbate and functional groups on the adsorbent. The interaction is stronger than the force of Van der Waals. This would occur on the adsorbent surface bearing active sites specific to the adsorbate. Therefore, the adsorbate molecules/ions adsorb on the surface only at these specific active sites and they are restricted from the migration due to high binding energy and heat of adsorption. Consequently, the adsorption occurs in monolayer regime and the process is irreversible.

2.3.1 Adsorption kinetics

Adsorption kinetics is used to evaluate the performance and to describe the adsorption behavior of the adsorbent. Moreover, the kinetics study is also used to design and develop the adsorption system. For the kinetic models, pseudo–first order and pseudo–second order are widely used for predicting the adsorption mechanism and calculating the kinetic parameters [43-45].

Pseudo-first order kinetic model

The pseudo-first order model is based on the amount of adsorbate on adsorbent at equilibrium and defined time. The model can be described by the equation 2.1 and after integration, a linear equation 2.2 is obtained,

$$\frac{dq_t}{dt} = k_1(q_e - q_t) \tag{2.1}$$

$$\log(q_e - q_t) = \log q_e - \frac{k_1}{2.303}t \tag{2.2}$$

where q_e is the amount of analyte adsorbed at equilibrium (mg/g),

q_t is the amount of analyte adsorbed at specific time (mg/g),

k_1 is the rate constant of pseudo-first order adsorption (min^{-1}),

t is adsorption time (min).

The value of k_1 and q_e can be calculated from the slope and intercept of the linear plotting of $log(q_e - q_t)$ versus time, respectively. If the $q_{e,cal}$ values are close to the values observed from the experiment ($q_{e,exp}$), it indicates that the kinetics of the studied adsorption process follows this kinetic model.

Pseudo-second order kinetic model

The pseudo–second order model assumes that the adsorption occurs through chemical adsorption. In this case, the adsorption rate is independent to concentration of adsorbate but it is dependent to the amount adsorbate on the adsorbent. The rate equation of the pseudo-second order model is given in equation 2.3 and the linear relationship is shown in equation 2.4,

$$\frac{dq_t}{dt} = k_2(q_e - q_t)^2 \tag{2.3}$$

$$\frac{t}{q_t} = \frac{1}{k_2 q_e^2} + \frac{t}{q_e} \tag{2.4}$$

where q_e is the amount of analyte adsorbed at equilibrium (mg/g),

q_t is the amounts of analyte adsorbed at time (mg/g),

k_2 is the rate constant of pseudo-second order adsorption (g/mg.min),

t is time (min).

From the linear plotting of t/q_t against time, the $q_{e,cal}$ and k_2 value are obtained from the slope and intercept, respectively.

2.3.2 Adsorption isotherms

Adsorption isotherms are used to describe the adsorption behavior at equilibrium. It involves the amount of adsorbate on adsorbent surface observed at equilibrium when the initial concentration is varied at constant temperature and pH. The isotherms were plot with between q_e and C_e. Moreover, the information of

these studies can be applied to design the treatment system. Different isotherm models are often applied to the experimental data to describe the adsorption behavior at equilibrium such as Langmuir, Freundlich, Temkin, and Dubinin and Radushkevich (DR) model [43, 45-51].

Langmuir isotherm

The Langmuir isotherm was developed by considering the interaction on the interface of solid–liquid phase. The adsorption mechanism is based on several assumptions including (i) the adsorbent has a homogeneous surface, suggesting that all active sites have relatively equivalent affinity towards the adsorbate and hence equivalent adsorption energy, (ii) the adsorption of the analyte occurs as monolayer on the surface, and (iii) the adsorption takes place at specific sites without the interaction between adsorbate ions/molecules on the surface. The Langmuir isotherm is shown in equation 2.5. The linear form is also demonstrated in equation 2.6,

$$q = \frac{q_m b C_e}{1 + b C_e} \tag{2.5}$$

$$\frac{C_e}{q} = \frac{1}{b q_m} + \frac{C_e}{q_m} \tag{2.6}$$

where C_e is the equilibrium concentration of analyte in aqueous solution (mg/L or mol/L),

q is the amount of analyte adsorbed on the adsorbent at equilibrium (mg/g or mol/g),

q_m is the maximum amount of analyte adsorbed or the maximum adsorption capacity of the adsorbent (mg/g or mol/g),

b is Langmuir constant related to the affinity of binding sites (L/mg or L/mol).

The value of q_m and b are obtained from the slope and intercept of the linear plot of C_e/q against C_e. In addition, the essential feature of Langmuir isotherm can be shown in term of separation factor constant (R_L) as follows [49].

$$R_L = \frac{1}{1+bC_i} \tag{2.7}$$

C_i is the initial concentration of arsenic in aqueous solution (mg/L). The parameter R_L determines the type of the isotherm and the meaning of R_L value is presented in Table 2.1.

Table 2.1 The R_L values and corresponding type of isotherm

R_L value	Type of isotherm
$R_L > 1$	Unfavorable
$R_L = 1$	Linear
$0 < R_L < 1$	Favorable
$R_L = 0$	Irreversible

Freundlich isotherm

The Freundlich isotherm model can be used to describe the adsorptions on the surface bearing various active sites or heterogeneous surface, according to the assumption that the adsorption sites have different binding affinity toward the adsorbate and hence, different binding energies. In addition, the adsorption may occur as multilayer adsorption and reversible. The Freundlich equation and its linear form are expressed in equation 2.8, and 2.9, respectively,

$$q = K_F C_e^{1/n} \tag{2.8}$$

$$\log q = \log K_F + \frac{1}{n} log C_e \tag{2.9}$$

where K_F is Freundlich constant related to adsorption capacity (mg/g or mol/g),

n is Freundlich constant related to adsorption intensity.

The linear equation obtained by plotting between $\log q$ versus $\log C_e$ can be used to calculate the K_F and n from the intercept and slope, respectively. When the value n parameter is higher than 1, it indicates that the sorption is favorable [45, 48].

Temkin isotherm

Temkin adsorption isotherm is used to describe the interactions between adsorbate and adsorbent that involve the heat of adsorption of molecules in the layer of adsorbate. It assumes that the heat of adsorption of all molecules decreases linearly when the surface of adsorbent is covered due to the adsorbate-adsorbent interactions. It also assumes a uniform distribution of binding energies up to some maximum binding energy. The linear form of Temkin model is shown in equation 2.10,

$$q_e = \frac{RT}{b}\ln A + \frac{RT}{b}\ln C_e \qquad (2.10)$$

where R is gas constant (8.31 J/mol K),

$\quad$ T is absolute temperature (K),

$\quad$ b is Temkin constant related to the heat of sorption (J/mol)

$\quad$ A is Temkin isotherm equilibrium binding constant (L/g).

The A and b parameters can be determined from linear plotting of q_e versus $\ln C_e$.

Dubinin and Radushkevich isotherm

Dubinin-Radushkevich (DR) model is applied to describe adsorption mechanism with a Gaussian energy distribution on heterogeneous surfaces. It is dependent on temperature. Typically, the model is used to determine type of adsorption between physical and chemical adsorption of analyte with its adsorption

energy, calculated from the isotherm plot. The Dubinin-Radushkevich (DR) isotherm is expressed in equation 2.11.

$$lnq_e = lnq_m - \beta\varepsilon^2 \qquad (2.11)$$

The adsorption potential or Polanyi potential (ε) can be calculated following equation 2.12. β is DR constant related the adsorption free energy (E) (mol^2/J^2).

$$\varepsilon = RTln(1 + \frac{1}{c_e}) \qquad (2.12)$$

$$E = \frac{1}{\sqrt{2\beta}} \qquad (2.13)$$

The linear equation was obtained by plotting $ln\ q_e$ against ε^2. The value of adsorption energy (E) can be used to determine the type of adsorption process as listed in Table 2.2.

Table 2.2 The E values that associate with the type of adsorption process [51]

Value of E (KJ/mol)	Type of adsorption process
E < 8	Physisorption
E = 8-16	Ion-exchange
E = 16-20	Chemisorption

2.4 Literature review

For arsenic removal from water by adsorption process, many types of material have been used. Among the available adsorbents for arsenic, biosorbents like chitosan have gained much attention due to its low cost, non-toxicity, biodegradability, and eco-friendly. Chitosan has been demonstrated as adsorbents for metal ions removal from aqueous solution due to the presence of amine groups on its structure. Herein, we focus on the removal of arsenic in water by chitosan as discussed as follows.

Gérente and coworkers [20] studied the removal of arsenate ions from contaminated water using chitosan flakes to observe the mechanism of adsorption. It was found that chitosan could adsorb arsenate through electrostatic attraction between positively charged amines on chitosan and anionic arsenate, which was a spontaneous reaction. The capacity of chitosan for arsenate adsorption was 1.37 mg/g at pH 5. The adsorption process fitted to Langmuir isotherm.

Kwok and coworkers [21] investigated the use of chitosan flakes and nanochitosan powders for removing arsenite and arsenate from aqueous solutions. The results showed that the capacity of chitosan for arsenite and arsenate adsorption at equilibrium was around 0.5 mg/g and 5 mg/g, respectively. While the capacity of nanochitosan for arsenite and arsenate adsorption was 6.1 mg/g and 13 mg/g, respectively. The initial pH was 6 and 4 for arsenite and arsenate adsorption, respectively. The capacities of both adsorbents for arsenate adsorption are higher than arsenite because arsenite existed in a neutral form, causing a lack of attraction on adsorption sites through electrostatic interaction. The nanochitosan powder showed a higher adsorption capacity because of its higher surface area, compared to chitosan flakes.

In addition, Kwok and coworkers [22] also studied the adsorption mechanism using chitosan flakes and nanochitosan powder for removing arsenate. The experiment results showed that the protonated amine groups of chitosan were observed in the pH range of 3.50-5.50 and the pH showed effect on the adsorption capacity. The interaction between the anionic arsenate and chitosan occurred via electrostatic attraction. From these results, the chitosan in form of flake or powder can remove arsenic from aqueous solution, but it has a low adsorption capacity.

From the review, it was found that the use of chitosan still has several drawbacks such as low stability in water, poor mechanical properties, low surface area, and low porosity. For chitosan in form of powder or flake, it causes clog or

difficulty in material separation from aqueous solution. Thereby, different chitosan composites have been fabricated to enhance its mechanical strength and the adsorption capacity and to suite their practical application. Several research are summarized hereafter as examples.

Charpentier and coworkers [33] prepared nanocomposite of chitosan and carboxymethylchitosan modified with magnetic nanoparticle for adsorption of Cu^{2+}, Pb^{2+}, and Zn^{2+} from contaminated water. The results showed that the capacity of the composites for metal ions adsorption was higher than that of chitosan-based adsorbent. The maximum adsorption capacity of the modified chitosan according to Langmuir isotherm was 141 mg/g for Pb^{2+}, 123 mg/g for Cu^{2+}, and 88 mg/g Zn^{2+}. Whereas the capacity of modified carboxymethylchitosan according to Freundlich isotherm was 243 mg/g for Pb^{2+}, 232 mg/g Cu^{2+}, 131 mg/g Zn^{2+}.

Su and coworkers [37] fabricated the zero-valent iron (nZVI)/chitosan composite foams (ICCFs) by freeze-drying method for removal of inorganic arsenic in water. It was found that the ICCFs exhibited porous structure with good mechanical property. The presence of zero-valent iron in the porous material improved the adsorption capacity to 114.9 mg/g for As(III) and 86.87 mg/g for As(V) at pH 6. The adsorption kinetics of As(III) and As(V) on ICCFs fitted well to the pseudo-second order and their isotherms followed Langmuir model. Furthermore, the performance of ICCFs on arsenic removal could be attributed to both its porous structure of chitosan and nZVI as active site for arsenic interaction.

Salih and coworkers [36] prepared a composite adsorbent by modifying chitosan with diatomite for removal of As(III) and As(V). The results indicated that the adsorption capacity of the material was enhanced with the maximum adsorption capacities of 87.81 mg/g and 44.07 mg/g for As(III) and As(V), respectively. These adsorptions could fit to Langmuir isotherm and pseudo-second order models.

Zhange and coworkers [25] fabricated an adsorbent for oil separation by incorporating nanofibrillated cellulose (NFC) into chitosan (CS) matrix through freeze-drying method. The CS/NFC adsorbent showed good mechanical performance due to the reinforcement of chitosan network structure with of NFC. Moreover, this material was stable in water and remained intact after being soaked for 30 days.

Abdul Khalil H.P.S and coworkers [26] collected and discussed about the properties and applications of the chitosan-cellulose/nanocellulose composites. It was found that the poor mechanical and thermal properties of chitosan have limited its applications. Thereby, the blending of chitosan with cellulose/nanocellulose could improve their mechanical properties. In addition, the cellulose/nanocellulose as reinforcement filler is eco-friendly. After blending, the composite can be used in many applications.

Geng and coworkers [27] prepared the composite of chitosan with different cellulose contents to observe the mechanical properties. The results showed that the chitosan composite had good mechanical properties, resulted from small amount of cellulose added to reinforce. This phenomenon could be explained by the interaction between chitosan and cellulose through H-bond formation and the cellulose could be dispersed homogeneously in chitosan matrix.

Zhang and coworkers [28] modified chitosan with cellulose, then crosslinked with glutaraldehyde. The sponge was obtained after freeze-dried and used for mercury(II) ions removal from aqueous solution. It was found that the chitosan/cellulose composite sponge (CCS) could adsorb Hg(II) ions rapidly and selectively. Besides, the CCS was easily separated from water compared with particulate or powder adsorbent. The adsorption capacity of 495 mg/g was obtained.

Chitosan/cellulose sponge has been demonstrated as a promising material for the adsorption application. Moreover, MOFs have received a lot of attention as material for arsenic adsorption. However, using MOFs may encounter the difficulty in

solid separation from water due to its small particle size. Herein, we used MIL-53(Fe) (MIL = Material Institute of Lavoisier) as a modifier in the chitosan/cellulose sponge due to its good chemical resistance, water stability, and ease of synthesis. The method of MIL-53(Fe) synthesis was investigated by Du and coworkers [31] and Yu and coworkers [32].

Furthermore, Vu and coworkers [38] synthesized MIL-53(Fe) using Fe^{3+} ions as the metal centers and terephthalic acid as organic ligands via solvothermal method for arsenic removal from aqueous solution. The results showed that the MIL-53(Fe) was successfully applied to remove arsenate from solution with the maximum adsorption capacity of 21.27 mg/g at pH < 6.9. The adsorption occurred through the complex formation of Fe-O-As as Lewis acid-base interaction between an anionic ligand of arsenate and the Fe^{3+} cations in the MIL-53(Fe). These adsorptions could fit with Langmuir isotherm and pseudo-second order models.

In this work, we are interested in the preparation of chitosan sponge reinforced with nanocellulose and modified with MIL-53(Fe) to improve the efficiency in arsenic removal.

CHAPTER 3

EXPERIMENTALS

3.1 Instruments

Table 3.1 List of analytical instruments

Instruments	Manufacturing/Models
Zetasizer Nano ZS (DLS)	Malvern
Fourier-transform infrared spectrometer (FT-IR)	Thermo Scientific/Nicolet iS50
X-ray diffractometer (XRD)	Rigaku/Smartlab
Transmission electron microscopy (TEM)	JOEL/JEM-2100
Scanning electron microscope (SEM)	JEOL/IT-100
Surface area analyzer	BEL Japan/BELSORP-mini
Inductively coupled plasma-optical emission spectrometer (ICP-OES)	Thermo Scientific/iCAP 6000 Series
Centrifuge	Cence/L500
Refrigerator	Mitsubishi/MR-F36J-GY
Freeze-dryer	LABCONCO
Teflon-line stainless-steel autoclave	PARR/Acid digest vess 125 mL
Oven	Memmert/UM 500
Vacuum pump	Millipore
Sonicator	Ultrasonic steri-cleaner
pH meter	Mettler TOLEDO/FiveEasy Plus
Shaker	Ratek/Orbital mixer incubator

3.2 Chemicals

All chemicals used in this research were of analytical grade and listed in Table 3.2.

Table 3.2 List of chemicals

Chemicals	Supplier
1,4-Benzenedicarboxylic acid (H_2BDC)	Merck
Acetic acid (CH_3COOH)	Merck
Acetone	RCI Labscan Limited
Arsenic standard solution	Merck
Cellulose microcrystalline (CMC)	Sigma-aldrich
Chitosan (CS)	Sigma-aldrich
Dimethylformamide (DMF)	RCI Labscan Limited
Ethanol	RCI Labscan Limited
Glutaraldehyde (GLU)	Sigma-aldrich
Hydrochloric acid (HCl)	Sigma-aldrich
Iron (III) chloride ($FeCl_3$)	Sigma-aldrich
Iron standard solution (1000 mg/L)	Merck
Magnesium sulfate ($MgSO_4$)	Fisher Scientific
Manganese (II) chloride ($MnCl_2.4H_2O$)	Kemaus
Mix metal standard solution (Sb, As, Be, Cd, Ca, Cr, Co, Cu, Fe, Pb, Li, Mg, Mn, Mo, Ni, P, Se, Sr, Tl, Sn, 100 mg/L of all chemicals)	Merck
N,N'-methylene bisacrylamide (MBA)	Sigma-aldrich
Nitric acid (HNO_3)	Merck
Sodium (meta) arsenite ($AsNaO_2$)	Sigma-aldrich
Sodium arsenate dibasic heptahydrate ($HAsNaO_4.7H_2O$)	Sigma-aldrich
Sodium hydrogen phosphate heptahydrate ($Na_2HPO_4.7H_2O$)	Panreac

Table 3.2 List of chemicals (continued)

Chemicals	Supplier
Sodium hydroxide (NaOH)	Merck
Sodium sulfate (Na$_2$SO$_4$)	Ajax Finechem
Urea	Merck

3.3 Methodology

3.3.1 Preparation of nanocellulose

Nanocellulose (NC) was synthesized from cellulose microcrystalline (CMC) powder by following the method reported by Shankar and Rhim [52] as described in Figure 3.1. The CMC powder (2 g) was dispersed in 48 mL of a solution containing 7% (w/w) NaOH and 14% (w/w) urea. The mixture was stirred at room temperature for a specific time before being frozen at -20℃ for another 2 h. After the mixture temperature reached room temperature, it was stirred for 10 min using a magnetic stirrer at 800 rpm. Then, the cellulose was washed with milli-Q water to eliminate excessive urea and NaOH, and separated by centrifugation at 3000 rpm for 10 min. The product was washed repeatedly until the pH of the runoff was around 7. After being freeze-dried, the nanocellulose powder was obtained. The effect of reaction time (1 – 4 h) was investigated.
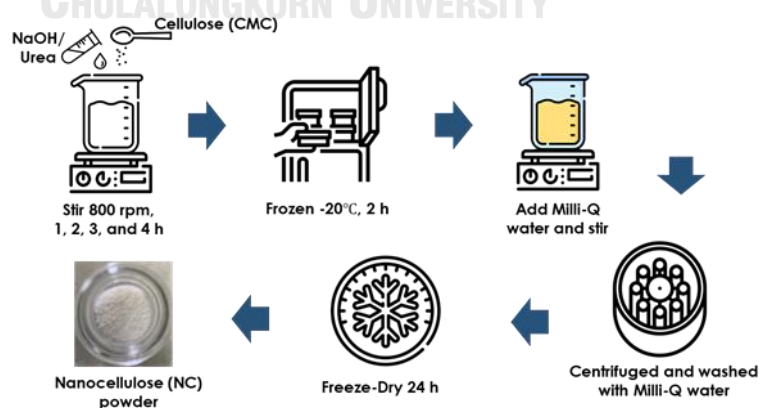
Figure 3.1 Schematic illustration of the synthesis of nanocellulose.

3.3.2 Synthesis of MIL-53(Fe) metal-organic framework

MIL-53(Fe) was prepared using the typical solvothermal process according to the previous work of Nguyen and co-workers [39]. $FeCl_3$ (1.35 g) and H_2BDC (0.83 g) were dissolved in 25 mL of DMF, stirred for 30 min at room temperature, and transferred to a Teflon-line stainless-steel autoclave. The mixture was heated at 150℃ for 6 h. After being left to cool down to room temperature, the solid was filtered and washed with 50% EtOH multiple times. Finally, the light orange powder was dried in an oven at 80℃ for 12 h as presented in Figure 3.2 and stored in a desiccator for later use.
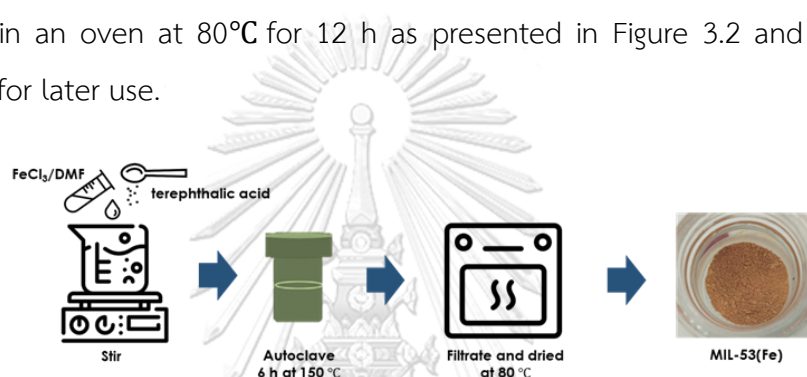
Figure 3.2 Schematic illustration of the synthesis of MIL-53(Fe) metal-organic framework.

3.3.3 Preparation of chitosan-nanocellulose composite material

For the preparation of CS-NC composite material, parameters affecting the sponge fabrication, the mechanical properties, and stability in water of the material such as chitosan (CS) content, nanocellulose (NC) content, amount of crosslinkers like glutaraldehyde (GLU) and N, N'-methylenebisacrylamide (MBA) were optimized.

Preliminary study

In this work, the CS was used as the main matrix to fabricate a sponge material for arsenic removal. CS was dissolved in 10 mL of 1% (v/v) acetic acid with various content at 0.5, 1.0, 1.5, 2.0, or 2.5% (w/w) to find the maximum content of CS that could be dissolved in this condition. The 2.0% (w/w) CS was used to fabricate

the sponge and glutaraldehyde (GLU) was added into the CS solution, stirred for 20 min, weighted in a vial approximately 1 g each and freeze-dried.

The effect of glutaraldehyde (GLU) concentration for crosslinking the CS was studied as shown in Table 3.3. The mechanical properties and stability in water of the obtained CS sponge was observed.

Table 3.3 The different glutaraldehyde concentration used in CS sponge preparation

Chitosan (% w/w)	Glutaraldehyde (% v/v)
	0.5
	1
2	3
	5
	10

Fabrication of chitosan-nanocellulose composite

Chitosan-nanocellulose composite (CS-NC) was prepared as presented in Figure 2.3. Firstly, a solution of CS and a NC suspension were prepared separately in 1% acetic acid solution. Secondly, CS solution and NC suspension were mixed and immediately stirred for 2 h to form a creamy homogeneous solution. Afterward, MBA crosslinker powder (if used) was added to the mixture, stirred for 20 min, and further sonicated for 30 min. Subsequently, 200 μL of GLU solution (if used) was put into the CS-NC solution dropwise under vigorous stirring. To acquire the mixture final weight of 20 g, an appropriate amount of 1% acetic acid solution was added. Then, the mixture was weighted in a vial approximately 1 g each and freeze-dried. The product in the vials were collected and kept for further use.
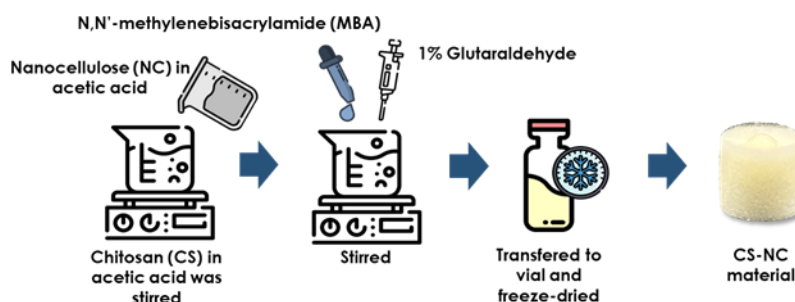
Figure 3.3 Schematic illustration of the synthesis of CS-NC composite.

The effect of N, N'-methylenebisacrylamide (MBA) concentration and GLU addition in CS-NC composite were studied using different conditions as presented in Table 3.4 (Entry 1 – 4). After curing, the obtained materials were tested for their stability in water, water uptake ratio, and mechanical properties and compared. The curing time was also observed.

Table 3.4 The different NC content reinforce in CS porous material

Entry	Chitosan (% w/w)	Nanocellulose (% w/w)	MBA (% w/w)	Glutaraldehyde (% v/v)
1	2	2	-	1
2	2	2	0.6	-
3	2	2	1.2	-
4	2	2	0.6	1
5	2	1	0.6	1

Effect of nanocellulose content

For investigating the effect of nanocellulose (NC) content for the CS-NC sponge preparation, the amount of NC was varied as 1 and 2 % as shown in Table 3.4 (Entry 4-5). After freeze-drying, the obtained materials were immediately tested for their stability in water and mechanical properties.

3.3.4 Preparation of CS-NC-MIL-53(Fe) composite

Effect of MIL-53(Fe) content

In the preparation of the CS-NC-MIL-53(Fe) composite (**Figure 3.4**), the mixture of 2 % CS and 1 % NC was prepared as described previously in the synthesis of the CS-NC composite. MIL-53(Fe) of specific amount was added into the CS-NC mixture to get a MIL-53(Fe) concentration of 0.5, 1.5, or 2.5% (w/w) and stirred for 2 h. An orange homogeneous suspension was obtained. Then, 0.6% (w/w) MBA powder and 200 µL of 1% GLU solution were added into the mixture before its final weight was adjusted to 20 g with 1% acetic acid solution. At this point, an orange viscous liquid suspension was obtained. the mixture was weighted in a vial approximately 1 g each and freeze-dried. The final products were washed with milli-Q water, rinsed with acetone to eliminate any remaining starting substances, and left to dry at room temperature. The obtained materials were tested for their stability in water and mechanical properties.
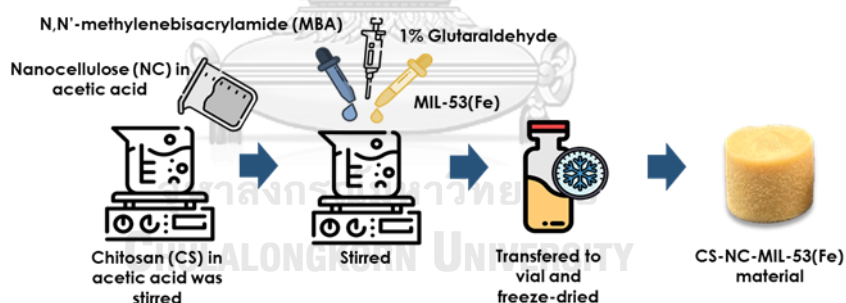
Figure 3.4 Schematic illustration of the synthesis of CS-NC-MIL-53(Fe) composite.

3.4 Characterization

The material characterization was performed to assert the success of the synthesis of the nanocellulose (NC), MIL-53(Fe), and the composites. Several techniques were used as described below.

3.4.1 Characterization of nanocellulose

The size and morphology of nanocellulose (NC) were determined by dispersing the material in milli-Q water before an analysis by dynamic light scattering (DLS) and transmission electron microscopy (TEM), respectively. To detect the functional groups on the materials, the samples were analyzed by Fourier transforms infrared spectrometry (FT-IR).

3.4.2 Characterization of MIL-53(Fe)

The crystalline structure and the functional group of MIL-53(Fe) were observed by powder X-ray diffraction (XRD) and FT-IR, respectively. Nitrogen adsorption by the materials was carried out to determine the surface area. The morphology of MIL-53(Fe) was observed by scanning electron microscope (SEM).

3.4.3 Characterization of composites

The unmodified and modified CS-NC composite were characterized by FT-IR, SEM, and nitrogen adsorption. The details of each technique are described as follows.

Fourier-transform infrared spectrometry

The functional groups on the CS-NC and CS-NC-MIL-53(Fe) composite materials were characterized by a FT-IR. The FT-IR spectra were recorded from 400 to 4000 cm^{-1} in attenuated total reflectance (ATR) mode.

Scanning electron microscopy

The surface morphology of the unmodified and modified composite materials was monitored by SEM. The samples were cross-sectioned and coated with Au before the analysis.

Surface area analysis

The surface area and pore size of the composite materials were determined by nitrogen adsorption analysis, and the adsorption data were fitted to Brunauer-Emmett-Teller (BET) model.

Energy dispersive X-ray spectroscopy (EDX) and elemental mapping analysis

The elemental composition of the CS-NC-MIL-53(Fe) adsorbent was determined by energy dispersive X-ray spectroscopy (EDX) and the distribution of elements on the material surface was observed by elemental mapping.

3.5 Water uptake study

The water uptake ability of the composite materials was evaluated. The dried composite materials were weighed and then, immersed in DI water for 180 min at room temperature. The wet weight of the sponge was determined by blotting the sponge with tissue paper to remove water adsorb on the surface and weighed immediately on an analytical balance. Then, the water uptake ratio of sponges in water calculated as follows:

$$\text{Water uptake ratio} = \frac{W_t - W_0}{W_0} \tag{3.1}$$

where W_0 is the weight of dried sponge (mg),

W_t is the weight of wet sponge at time (mg).

3.6 Adsorption study

The adsorption of arsenic in aqueous solutions by the composite material was studied. In this research, a piece of adsorbent (*ca.* 40 mg) was added into 20 mL of the solution containing As(III) or As(V) and shaken at 100 rpm for 12 h. The concentration of As(III) or As(V) solution before and after the adsorption was determined by an inductively coupled plasma optical emission spectrometer (ICP-OES). The adsorption capacity (q, mg/g) and the efficiency of the composite material for arsenic removal were calculated using equations 3.2 and 3.3, respectively;

$$q = \frac{(C_i - C_f)}{m} \times V \tag{3.2}$$

$$\text{Removal (\%)} = \frac{(C_i - C_f)}{C_i} \times 100 \tag{3.3}$$

where C_i is the initial concentration of arsenic in solution (mg/L),

C_f is the final concentration of arsenic in solution (mg/L),

m is the mass of composite material used in the adsorption (g),

V is the volume of arsenic solution (L).

Furthermore, the arsenic standard solution (1000 mg/L) was used to prepare arsenic standard solutions of desired concentrations by diluting the solution with milli-Q water. The arsenic stock solutions for the adsorption experiments were freshly prepared by dissolving a specific amount of $AsNaO_2$ or $HAsNaO_4.7H_2O$ in milli-Q water. And the nitric acid solution (1 %v/v) was prepared by direct diluting the concentrated solution (65%) in milli-Q water for ICP-OES analysis.

3.6.1 Effect of initial pH of the arsenic solution

The effect of initial solution pH on arsenic adsorption efficiency of composite material was investigated in a pH range from 3 to 11. The initial concentration of arsenic was 40 mg/L and the contact time of 12 h was adopted. The initial pH of the solutions was adjusted to the desired value using HCl or NaOH solution.

3.6.2 Effect of contact time

The effect of contact time on arsenic adsorption by composite material was investigated using a piece of adsorbent and 20 mL of the arsenic solution having an initial pH was 9 for As(III) and As(V). The initial concentration used was 40 mg/L for As(III) and As(V). The contact time was varied in the range of 0.5 to 15 h.

3.6.3 Effect of initial concentration (Adsorption isotherm)

The adsorption experiments were performed under controlled temperature at 25°C. The initial concentration of the arsenic solution was varied in the range of 5-50 mg/L and 20-175 mg/L for As(III) and As(V), respectively. The initial of pH solutions was 9 and contact time was fixed to 12 h. The obtained data were fit to the Langmuir, Freundlich, Temkin, and Dubinin and radushkevich (DR) isotherm model to study the adsorption behavior of the materials.

3.6.4 Effect of interfering ions

The effect of anions, cations, and heavy metal ions other than As(III) and As(V) was studied in a binary mixture system. For each mixture, it contained 0.4 mM As(III) or 0.8 mM As(V) and other individual species. The ions studied included PO_4^{3-} and SO_4^{2-} as anion, Na_2SO_4 and $MgSO_4$ as salts of different cations, and Cr(VI), Mn(II), Fe(III), Ni(II), Cu(II), Zn(II), Cd(II), and Pb(II) as heavy metal ions. The concentration of the studied interfering ions was 0.4 or 4.0 mM for the adsorption of As(III) and 0.8 or 8.0 mM for the adsorption of As(V).

3.7 Application to real water sample

The real wastewater sample used in this study was collected from a petroleum refining industry at Rayong province (Thailand). Before use in this

experiment, the wastewater was analyzed for the concentration of total arsenic by ICP-OES and the pH was also measured.

The sample solution from the first source had the pH and arsenic concentration about 9.2 and 4.09 mg/L, respectively. Meanwhile, the second source sample had the pH value of 6.8 and arsenic concentration of about 736.02 mg/L. The sample that contained high concentration of arsenic was diluted with milli-Q water 20 times and adjusted sample pH to 9. The CS-NC-MIL-53(Fe) composite materials were used to remove the arsenic in 20 mL of wastewater with a contact time of 12 h. Moreover, different doses of adsorbent (1, 2, and 3 pieces) were added in the sample water to adsorb arsenic. Afterward, the residual concentrations of arsenic in two sources were determined.

CHAPTER 4

RESULTS AND DISCUSSION

4.1 Preparation and characterization of nanocellulose

In the nanocellulose (NC) preparation, the reaction time for size reducing from crystalline microcellulose (CMC) to NC was optimized. The obtained nanocellulose from different conditions were characterized by DLS, TEM, and FT-IR.

4.1.1 Effect of time

In this process, the preparation of NC particles from CMC was carried out using NaOH/urea solution with different reaction time ranging from 1 h to 4 h under continuous stirring at 800 rpm. After freeze-drying, the final product was obtained as white and lightweight powder. The impact of time in the NC preparation was observed using dynamic light scattering for size determination.

4.1.2 Characterization of nanocellulose
Dynamic light scattering (DLS)

The results of DLS analysis could reveal the average particle size and the polydispersity index (PDI) of NC obtained as presented in Table 4.1 and Figure 4.1. The NC particles size was smaller with increasing time and low PDI values was observed (0.3-0.6). It suggested that an inter- and intra-hydrogen bonds between cellulose molecules were destroyed resulting in the reduction of particle size with low particles size distribution (PDI < 0.7) [53-56]. Consequently, the specific surface area and water sorption of cellulose increased, which was suitable for the composite preparation. Although the stirring time was prolonged from 2 h to 4 h, the sizes were still around 400 nm and not remarkably changed. Therefore, the time for NC

preparation from CMC of 2 h was chosen to save time as it was sufficient for producing NC of desired size.

**Table 4.1** Size and PDI of NC particles obtained using different magnetic stirring times

Time (h)	Size (nm)	PDI
1	540.4 ± 9.5	0.583
2	433.5 ± 41.0	0.442
3	414.7 ± 38.7	0.407
4	371.4 ± 15.9	0.359
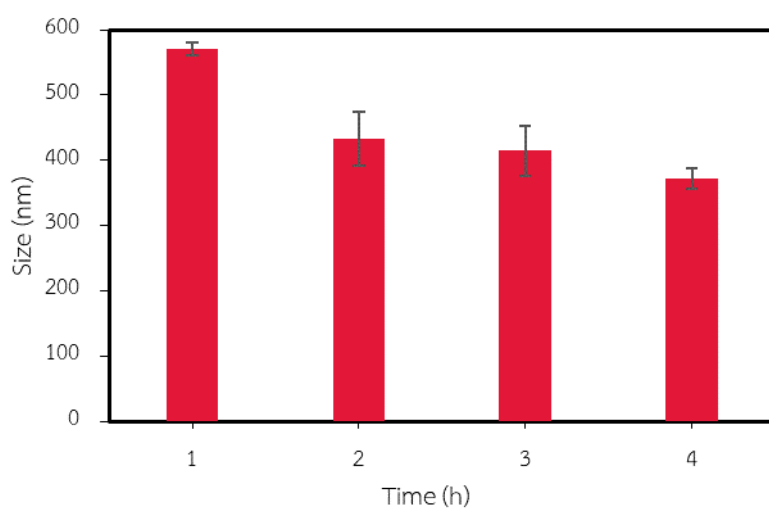
Figure 4.1 The effect of time for NC preparation on the obtained NC size

Transmission electron microscopy (TEM)

To observe the morphological structure of the NC obtained, the dispersed NC was analyzed by the TEM as shown in Figure 4.2.
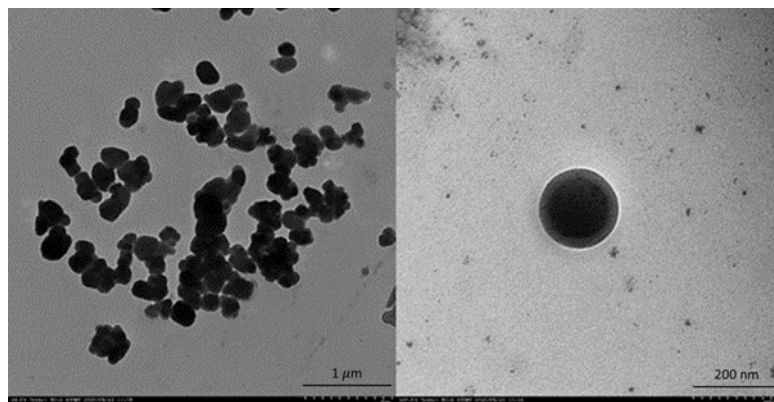
Figure 4.2 TEM images of the prepared NC.

The images show that the prepared NC were in spherical shape with the size in the range of 135.8 – 177.8 nm. The particle sizes measured by TEM and DLS methods were remarkably different. This is because the TEM determined the physical size of particles in their dried form, while the DLS analyzed the particles dispersed in an aqueous solution. As NC is highly hydrophilic and it would swell in water, hence, their particles size determined by DLS method was likely to be larger.

Fourier transform infrared (FT-IR) spectroscopy

The functional groups present in CMC and synthesized NC were studied by FT-IR as shown in Figure 4.3. The IR spectra were recorded using ATR mode.
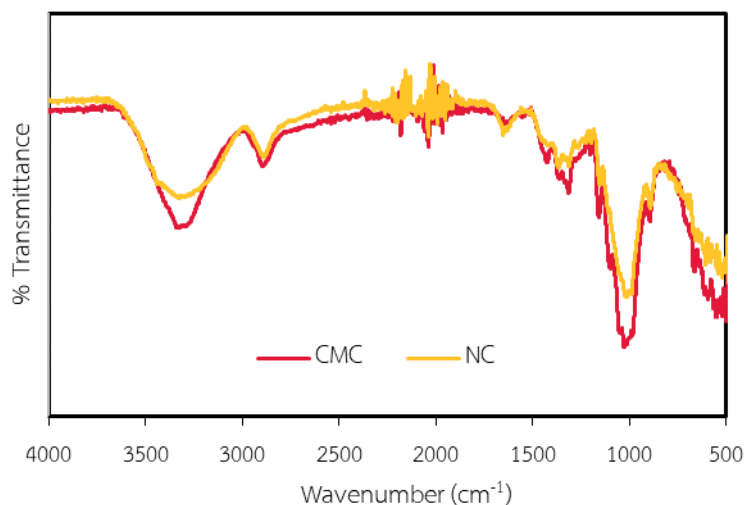
Figure 4.3 FT-IR spectra of CMC and NC.

The main characteristic peaks are listed in Table 4.2, which corresponded to the chemical structure of cellulose. It was reported that the change in the crystalline structure of cellulose leads to a disappearance or a reduction in intensity of certain FT-IR peaks of the crystalline domains of cellulose [57]. In this study, the results showed that the intensity of the peak at 1429 cm^{-1} of the NC crystalline was significantly lower than that of CMC. Owing to a destruction of hydrogen bonds in the synthesis process, the crystallinity decreases [54-56]. All the characterization results confirmed that NC was obtained.

**Table 4.2** The main characteristic peaks and assigned functional groups of NC observed by FT-IR

Wavenumber (cm^{-1})	Functional group
3389	-OH stretching
2890	C-H stretching
1429	$-CH_2$ bending
1053	C-O-C stretching

4.2 Synthesis and characterization of metal-organic framework MIL-53(Fe)

MIL-53(Fe), used to modify the nanocellulose-chitosan composite, was synthesized by using the method proposed by Nguyen and co-workers [39]. The obtained materials were characterized by XRD, FT-IR, surface area analysis, and SEM.

X-ray diffraction (XRD)

X-ray diffraction was used to characterize the crystallinity of the obtained MIL-53(Fe). The XRD pattern of MIL-53(Fe) is shown in Figure 4.4. The material showed a highly crystalline structure with main diffraction peaks at 9.4°, 12.58°, 18.84°, and 21.98°. The results of the prepared MOF agreed well with those of MIL-53(Fe) observed in the previous work [49, 50].
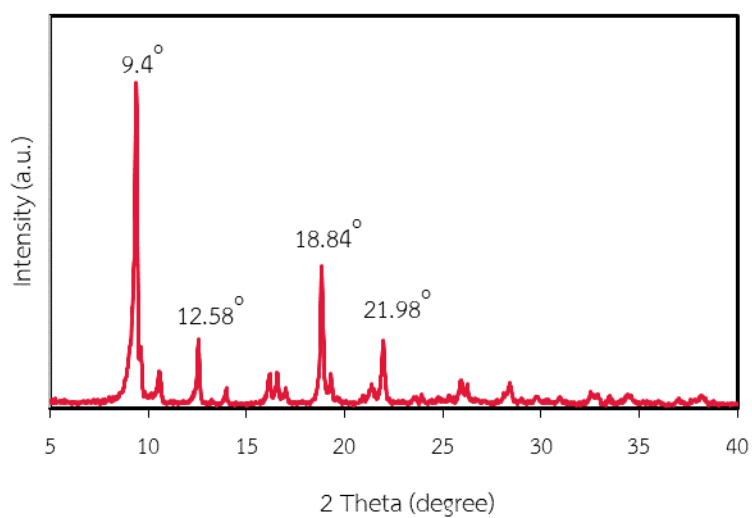
Figure 4.4 XRD pattern of the prepared MIL-53(Fe) metal-organic framework.

Fourier transform infrared (FT-IR)

The FT-IR spectra of MIL-53(Fe) is displayed in Figure 4.5 and several characteristic peaks and the expected functional groups of MIL-53(Fe) are listed in Table 4.3. The characteristic coordination between Fe^{3+} cation and $-OOC-C_6H_4-COO-$ carboxylate anions of the ligand in the structure of MIL-53(Fe) was confirmed by Fe-O stretching located at 522 cm^{-1} [38, 40]. The other signals belonged to the terephthalic acid ligand were observed at 1660, 1588, 1382, and 748 cm^{-1}, reflecting the presence of the aromatic group and dicarboxylic linker. These characterization results revealed that MIL-53(Fe) crystal was obtained.
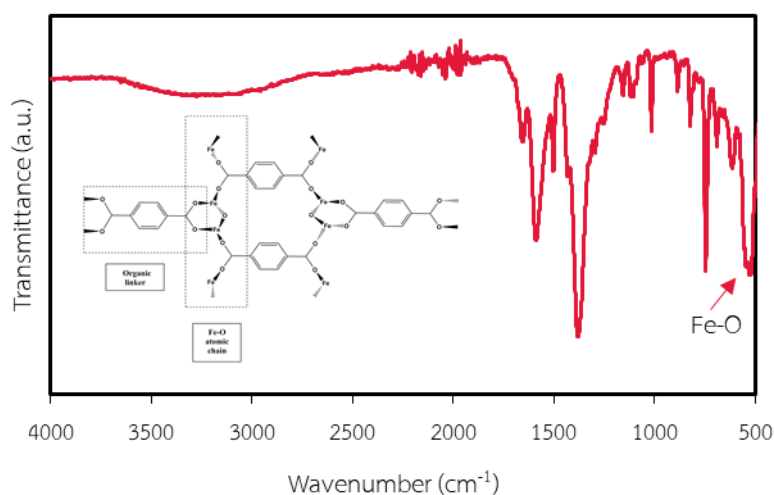

Figure 4.5 FT-IR spectra of MIL-53(Fe) metal-organic framework.

Table 4.3 The main characteristic peaks and assigned functional groups of MIL-53(Fe) observed by FT-IR

Wavenumber (cm^{-1})	Functional group
1660	C=O
1588	Asymmetric C-O
1382	Symmetric C-O
748	C-H bending
522	Fe-O stretching

Surface area analysis

The specific surface area of as-prepared MIL-53(Fe) was determined by N_2 adsorption - desorption isotherms at 77 K and the results are shown in Figure 4.6. The N_2 adsorption - desorption curves displayed an intermediate mode between type I and IV isotherms, which corresponded to the adsorption inside micropores and mesopores, respectively [38]. The Brunauer-Emmett-Teller (BET) surface area and total pore volume of the MIL-53(Fe) were calculated to be 22.139 m^2 g^{-1} and 0.036 cm^3 g^{-1}. The results revealed that the prepared MIL-53(Fe) was not a porous material, and hence it exhibited low specific surface area [58, 59].
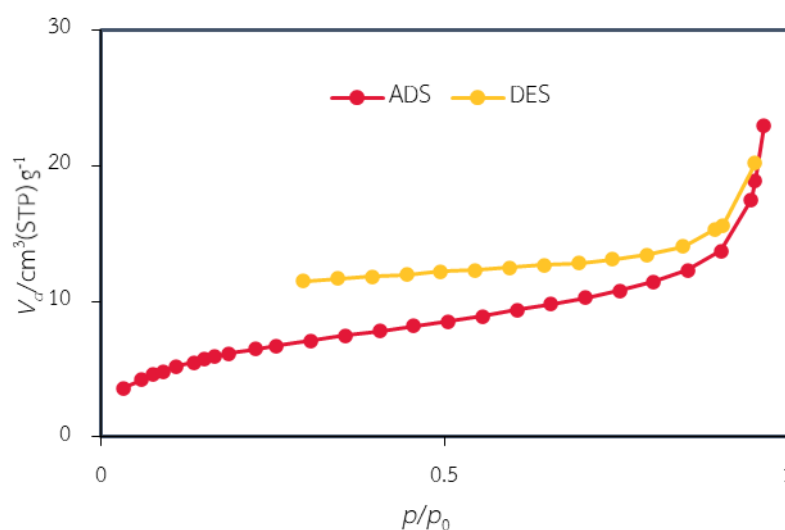
Figure 4.6 Nitrogen adsorption – desorption isotherm of MIL-53(Fe).

Scanning electron microscope (SEM)

The morphology and size of the as-synthesized MIL-53(Fe) were observed by SEM as shown in Figure 4.7. The MIL-53(Fe) frameworks exhibited the octahedron-like crystalline structures of different sizes. The surface of MIL-53(Fe) crystals displayed smooth surface, which is consistent with that reported in the literature [38, 39].
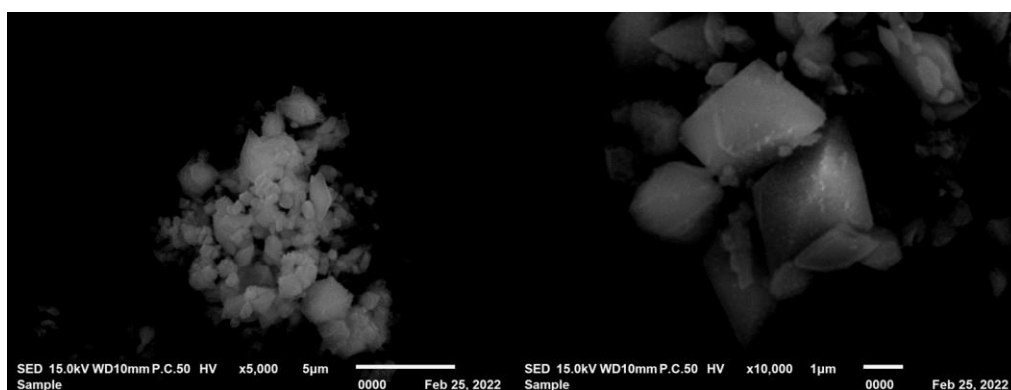

Figure 4.7 SEM image of MIL-53(Fe).

The results from all the characterization techniques confirmed the successful synthesis of MIL-53(Fe). The MIL-53(Fe) was further used in the modification of chitosan-nanocellulose composite material for removing arsenic in aqueous solutions.

4.3   Preparation   of   chitosan-nanocellulose   composite   material   and characterization

In the synthesis of chitosan-nanocellulose composite material, the factors that affected the sponge fabrication, including chitosan (CS) concentration, nanocellulose (NC) content, and amount of crosslinker i.e. glutaraldehyde (GLU) and N, N'-methylenebisacrylamide (MBA) were optimized regarding the mechanical properties and stability in water of the obtained sponge.
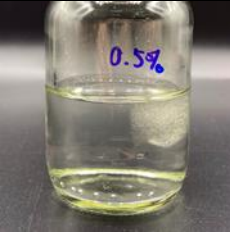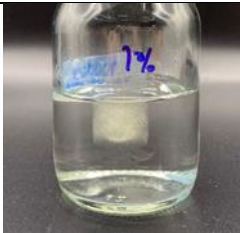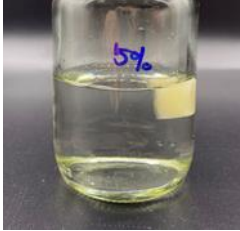
4.3.1 Preliminary study

The CS content in the composite would affect the mechanical properties, water stability, and adsorption properties of the composite. The amine groups ($-NH_2$) on the CS chain were active sites for arsenic adsorption, enhancing the adsorption efficiency of the composite. In this experiment, CS was dissolved in 1% (v/v) acetic acid solution with different CS content varied as 0.5, 1.0, 1.5, 2.0, and 2.5% (w/w). It was found that the solutions containing CS up to 2.0% (w/w) were homogeneous and CS were completely dissolved, while heterogeneous mixture was obtained in the preparation of 2.5% (w/w) CS due to an incomplete dissolution of CS. Therefore, the maximum CS concentration (2.0% w/w) was used to prepare the material due to the high amine ($-NH_2$) content for arsenic adsorption.

In the fabrication of CS sponge, glutaraldehyde (GLU) is commonly used as crosslinker to connect the chain of CS to improve the mechanical properties and stability in water without material deformation. By using 2% (w/w) chitosan, the concentration of GLU was varied in a range from 0.5 – 10% (v/v) (Table 4.4). The crosslinking was performed by adding 200 μL of GLU into 20 mL of the CS solution under vigorous stirring before transferring the mixture to vials for freeze-drying. Then, stability in water test was carried out with the obtained materials to find a suitable GLU concentration for future use in the CS-NC composite preparation.

Table 4.4 The effect of glutaraldehyde concentration in CS sponge preparation

Chitosan (% w/w)	Glutaral-dehyde (% v/v)	Liquid mixture appearance	CS sponge appearance	Stability in water
2	0.5	2CS-0.5GLU	2CS-0.5GLU	2CS-0.5GLU

	1	2CS-1GLU	2CS-1GLU	2CS-1GLU
	3	2CS-3GLU	2CS-3GLU	2CS-3GLU
	5	2CS-5GLU	2CS-5GLU	2CS-5GLU
	10	2CS-10GLU	-	-

To fabricate a sponge from CS, the CS should be partially crosslinked to improve the mechanical properties and stability in water. From the results, it was found that the CS solution color turned darker yellow by increasing the glutaraldehyde concentration. However, the CS solution formed a gel after adding 10% (v/v) GLU, indicating that a high degree of crosslinking occurred. On the other hand, by using 0.5, 1, 3 and 5% (v/v) GLU, CS sponge could be beautifully formed. The CS sponges crosslinked with 3 and 5% (v/v) GLU demonstrated a good stability in water. However, these materials were rarely swelled in water and easily broken

when squeezed. This could be explained by a relatively high degree of crosslinking occurred under these conditions, resulting in a more rigid structure, a relatively low free amine (-NH$_2$) groups left on the polymer, and hence, less hydrophilicity. In contrast, by using 0.5 and 1% (v/v) GLU, the materials were stable in water with a good swelling. Moreover, these materials exhibited a good mechanical property as evidenced by physical testing by pinching and squeezing. When soaking both sponges for a long time (> 12 h), it swelled more, risking of breaking, especially the sponge with 0.5% (v/v) GLU due to lower degree of crosslinking. Although, the GLU crosslinker could improve the stability of CS composite material in water, the material did not show good mechanical properties. Therefore, NC was further added into the CS to improve the mechanical properties of the material with and without using 1 %(v/v) GLU. The effect of cellulose crosslinker (i.e. N, N'-methylenebisacrylamide, MBA) was also investigated in the formation of CS-NC composite.
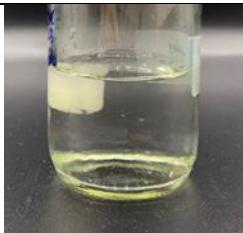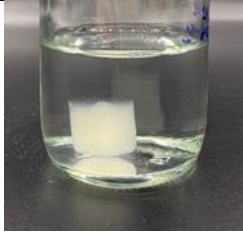
4.3.2 Formation of CS-NC composite sponge

In this study, 2% (w/w) CS concentration was chosen to fabricate the sponge and blended with NC of the same concentration (2 % w/w) to reinforce the material and improve the mechanical properties. The effect of crosslinkers addition and crosslinkers content were investigated. 1% GLU was adopted from the previous study, while the MBA concentration was varied from 0 – 1.2%. The results are shown in Table 4.5. The materials were named after the components used in the synthesis including their concentrations. The stability of materials in water was tested by immersing the material in water for 12 h and then the physical appearance, mechanical properties, and water uptake ratio (at 180 min) were observed.

From our preliminary study, the composite sponge 2CS-2NC without using any crosslinkers required a curing time of 2 months to be stable in water. Otherwise, it

broke when immersed immediately in water after freeze-drying. To overcome these drawbacks, MBA and GLU crosslinkers were required. The investigations started with using each crosslinker in the composite sponge fabrication, and then compared to the combination of the crosslinkers.

Table 4.5 The condition for fabrication of CS-NC composite material and material properties

CS-NC (% w/w)	MBA (% w/w)	GLU (% v/v)	Material curing time	Water uptake ratio (180 min)	Observed properties
2 % CS 2 % NC	-	1	-	39.94	2CS-2NC-1GLU
	0.6	-	5 days	30.40	2CS-2NC-0.6MBA
	1.2	-	5 days	27.52	2CS-2NC-1.2MBA
	0.6	1	-	24.70	2CS-2NC-0.6MBA-1GLU

It was found that the CS-NC composite obtained by using only GLU crosslinker showed good stability in water after freeze-drying and good mechanical properties resulted from NC reinforcement. The material showed high water uptake, probably due to the structure that could adsorb a lot of water. Nevertheless, this structure flexibility still needed to be improved.

Meanwhile, sole MBA crosslinker was used to improve the composite mechanical properties instead of GLU and was investigated to maintain the amine groups on CS as active sites for arsenic removal. In this case, MBA was mixed with CS-NC solution to obtain an MBA concentration of 0.6 or 1.2% (w/w) without GLU addition. The results showed that the **2CS-2NC-0.6MBA** and **2CS-2NC-1.2MBA** composites were not ready for the immediate use after freeze-drying, they had to be cured for 5 days for the structure to be stable in water. However, by using MBA, the curing time decreased from 2 months to 5 days. Moreover, the properties of materials prepared with 0.6 and 1.2% (w/w) MBA were not remarkably different, but the material with 0.6% (w/w) MBA had slightly higher water uptake ratio. This observation may be explained by the presence of hydrophilic chitosan as the main matrix of the composite. It should be noticed that the water uptake by the materials crosslinked with MBA was lower than that crosslinked with GLU. The composite material structures were denser when the NC in the composite were crosslinked with MBA. However, the requirement of curing time was the major drawback of this condition and therefore, GLU was further used in combination with MBA to fabricate CS-NC composites.

In the last condition, 1% w/w GLU and 0.6% w/w MBA were added to crosslink 2% CS and 2% NC in the composite fabrication. The 2CS-2NC-0.6MBA-1GLU material exhibited good mechanical properties and its form restored rapidly after being squeezed due to a good flexibility. The phenomenon may be resulted from the suitable degree of crosslinking that interconnected the network of CS chain incorporated with crosslinked NC to give rise to network elasticity and strength.

Moreover, the efficiency of 2CS-2NC-1GLU and 2CS-2NC-0.6MBA-1GLU composite in arsenate removal was examined as shown in Figure 4.8. Both composite materials showed similar arsenate removal efficiency, indicating that the addition of MBA did not affect the arsenic removal as it depended on amine groups of CS. It also revealed that the difference in water uptake of these two materials did not affect their adsorption ability. Thus, this condition with MBA addition was further applied to fabricate CS-NC composite sponge.
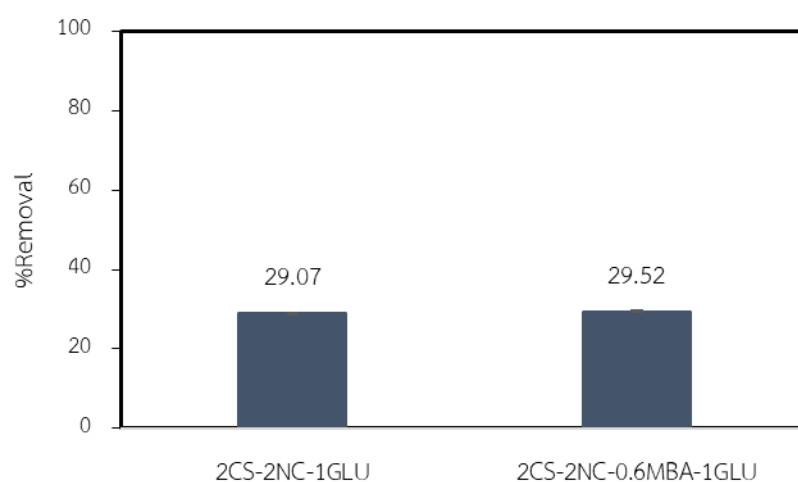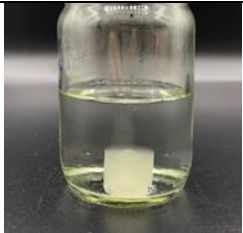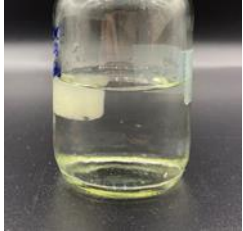
Figure 4.8 Efficiency of arsenate removal by 2CS-2NC-1GLU composite compared to 2CS-2NC-0.6MBA-1GLU (initial concentration of 20 mg/L As(V), pH 5, 12 h).

4.3.3 Effect of nanocellulose content

In this study, NC was added into the composite to enhance the mechanical strength by reinforcement. However, high content of NC would lead to a dense structure and hence, suitable content of NC should be used. In this experiment, NC were mixed with chitosan solution to obtain a NC concentration of 1 or 2 % w/w. Then MBA was added and followed by GLU to crosslink NC and CS before freeze-drying. Their water stability and ability in arsenate adsorption were investigated as presented in Table 4.6 and Figure 4.9, respectively.

Table 4.6 The effect of NC content on the property of CS-NC composite sponge

Chitosan (% w/w)	Nanocellulose (% w/w)	MBA (% w/w)	Glutaraldehyde (% v/v)	Stability in water
2	1	0.6	1	2CS-1NC-1GLU
	2			2CS-2NC-1GLU

From the experiment, it was found that all the materials were stable in water. The composite materials were kept in water for 12 h, these materials had a good water stability, good swelling, good mechanical property, which was clearly evidenced as it restored the original form quickly after being squeezed. For the effect of NC content, both of conditions did not clearly show difference in the strength of material. When the materials were used to adsorb arsenate, the results indicated that the different amount of NC in the composites did not affect arsenate adsorption. As NC may interact with CS through hydrogen bonding, hence, there was plenty of amine groups available as active sites in the composite for anionic arsenate adsorption. Therefore, 2CS-1NC condition was chosen to economize on starting material usage.
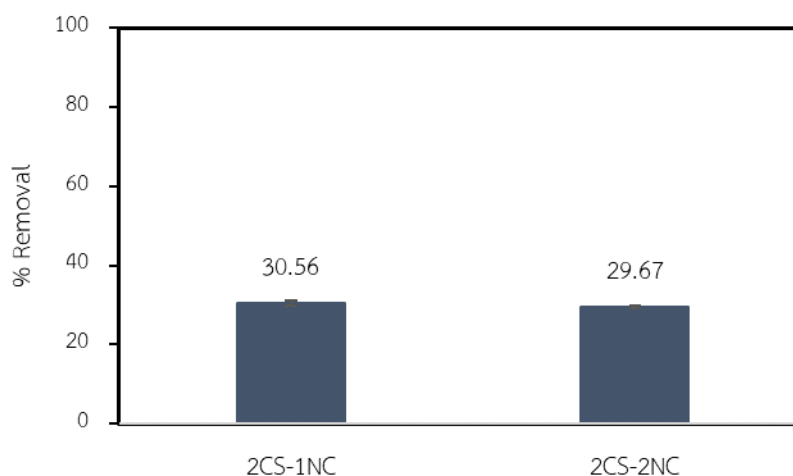
Figure 4.9 Efficiency of arsenate removal by 2CS-1NC and 2CS-2NC composite(initial concentration of 40 mg/L As(V), pH 5, 12 h).

4.3.4 Characterization of CS-NC composite

Fourier-transform infrared spectroscopy (FT-IR)

The FT-IR technique was used to characterize the CS-NC composite material compared with pure CS and NC as shown in Figure 4.10. The results of CS-NC composite material analysis showed a broad characteristic peak at 3350 cm^{-1}, attributed to the -OH and -NH$_2$ stretching vibrations, which were the characteristic peaks of NC and CS. The peak at 1655 cm^{-1} was related to the C=O stretching vibration of amide-I (-NHCOCH$_3$) of CS. In this region, the formation of C=N bond from the crosslinking reaction between -NH$_2$ groups of CS and -CHO groups of GLU in the composite material was also observed [28]. The peak at 1540 cm^{-1} was assigned to the N-H bending vibrations from -NH$_2$ groups of CS component. In addition, other characteristic peaks at around 2847 cm^{-1}, 1381 cm^{-1}, and 1025 cm^{-1}, belonged to the C-H stretching, -CH$_2$ bending, and asymmetric stretching of C-O-C bridge, respectively [60, 61]. These results demonstrated that the CS-NC composite material was successfully synthesized.
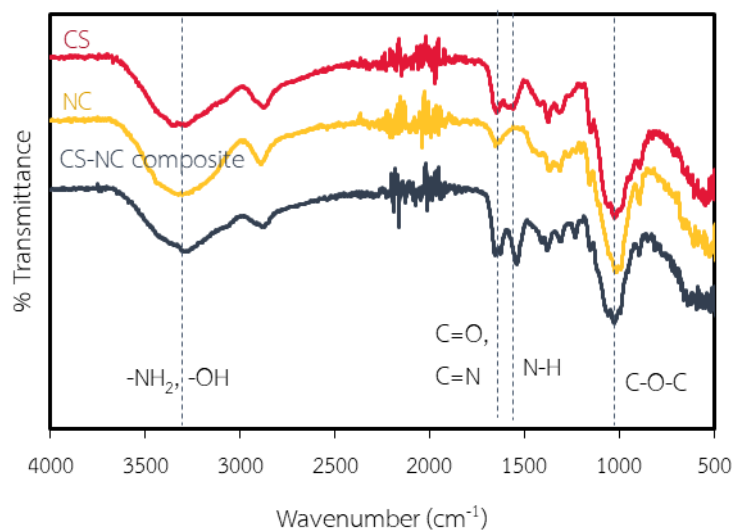
Figure 4.10 FT-IR spectra of CS-NC composite material compared with pure CS and NC.

Surface area analysis

The specific surface area of the fabricated CS-NC composite material was investigated by nitrogen adsorption analysis and compared with CS powder and CS porous material. The results are shown in Table 4.7.

Table 4.7 Surface area of materials

Material	Surface area (m^2/g)
CS powder	3.21
CS porous material	8.67
CS-NC porous material	5.96

The results showed an increasing specific surface area in CS porous material compared to CS powder due to the porosity of the material obtained by freeze-drying method. For the CS-NC composite material, the surface area declined to 5.96

m^2/g probably due to the distribution of NC particles in the structure, lowering the porosity of CS-NC composite.

Scanning electron microscopy (SEM)

The analysis of the cross-section CS-NC composite material by SEM revealed some features about the texture and morphology of the material as shown in Figure 4.11. These images showed a porous structure with different pore sizes in the range of micrometer-diameter, which may be caused by the irregular growth of ice crystal during the freeze-drying process leading to the formation of porous structures. By comparing the CS and CS-NC composite materials, CS-NC composite material had slightly larger pores. The NC component in the composite would interact with CS through H-bonding and hence distribute homogenously throughout the composite material. Consequently, the pore formation in the composite obtained after freeze-drying process were different from that of pure CS. The surface CS material were smooth, while the image of CS-NC composite revealed some particles deposited on the surface, which were probably the NC particles (Figure 4.11c, d). The results from FT-IR, surface area analysis, and SEM confirmed the successful synthesis of the CS-NC composite material.
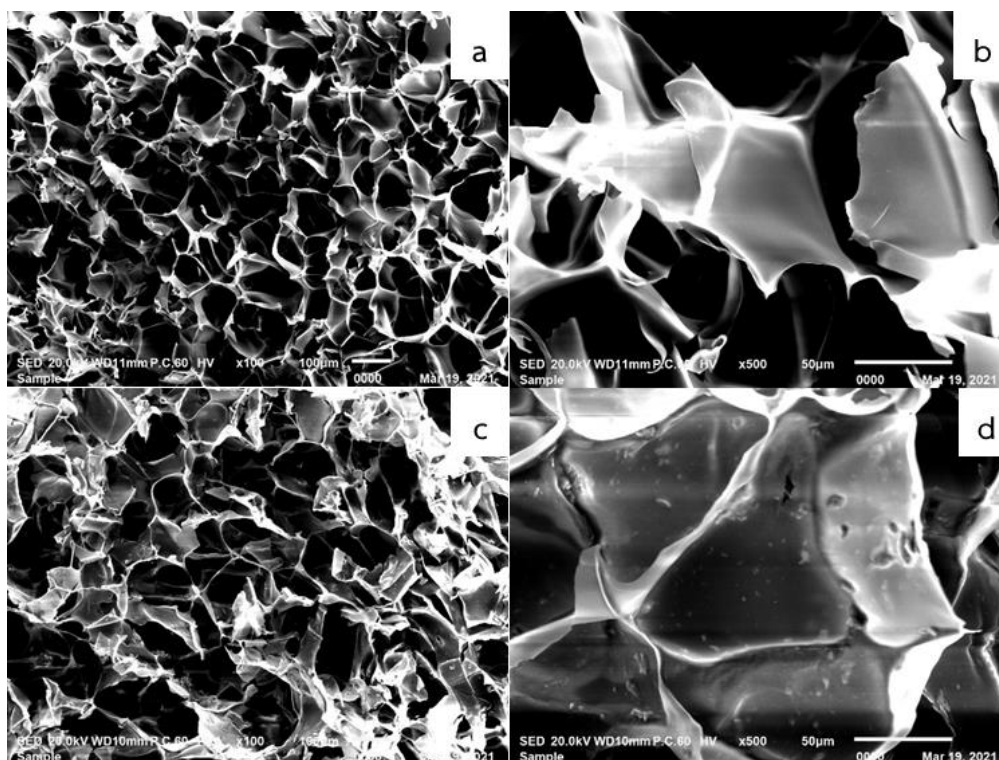
Figure 4.11 SEM images of (a, b) CS sponge and (c, d) CS-NC composite material.

4.4 Preparation of CS-NC-MIL-53(Fe) composite material and characterization
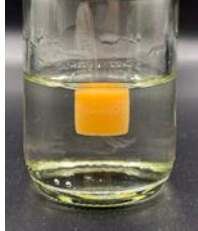
The most suitable conditions for the fabrication of CS-NC composite material were adopted in this study. The composites were further modified with MIL-53(Fe) to improve the adsorption capacity toward arsenic species. The materials were prepared and characterized as followed.

4.4.1 Effect of MIL-53(Fe) content

In this process, the CS-NC composite mixture was prepared following above-mentioned condition. The MIL-53(Fe) solid was added into the composite mixture with different MIL-53(Fe) contents as 0.5, 1.5, or 2.5 % (w/w) of the system as presented in Table 4.8. It was observed that the composite materials color turned to darker apricot with increasing MIL-53(Fe) content. The CS-NC composite with 0.5 and

1.5% (w/w) MIL-53(Fe) were stable in water and showed good mechanical property after soaking for 15 h as the example in Figure 4.12. However, the composite prepared with a high content of MIL-53(Fe) as 2.5 %(w/w) deformed due to an excessive amount of MIL-53(Fe) in chitosan matrix that caused easy breakage. Therefore, the conditions of 0.5 and 1.5% (w/w) MIL-53(Fe) for the CS-NC composite preparation were further used.

Table 4.8 The component conditions of CS-NC-MIL-53(Fe) materials and its properties

CS (%w/w)	NC (%w/w)	Glu (%v/v)	MBA (%w/w)	MIL-53(Fe) (%w/w)	Physical appearance	Stability in water
2	1	1	0.6	0.5	2CS-1NC-0.5 MIL-53(Fe)	
				1.5	2CS-1NC-1.5 MIL-53(Fe)	
				2.5	2CS-1NC-2.5 MIL-53(Fe)	-
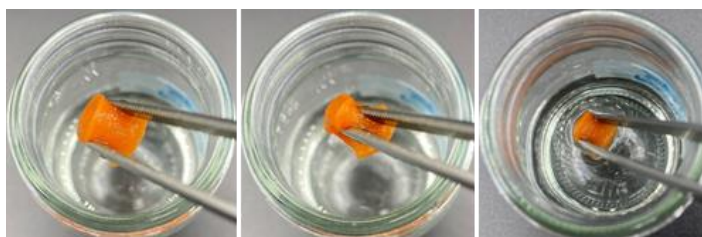
Figure 4.12 The mechanical property test of 2CS-1NC-1.5MIL-53(Fe)

when immersed in water.

The 2CS-1NC-0.5MIL-53(Fe) and 2CS-1NC-1.5MIL-53(Fe) composites clearly exhibited higher efficiency in arsenic removal than CS-NC composite as shown in Figure 4.13. Since the MIL-53(Fe) crystals acted as the adsorptive site of arsenic through coordination. The removal efficiency of arsenic increased up to 69.30 and 98.24% for As(III) and As(V), respectively with increasing the amount of MIL-53(Fe) to 1.5% (w/w). The results suggested that the increasing arsenic removal caused from collaboration between active sites of CS and MIL-53(Fe). As the results, the suitable weight ratio for the composite preparation was 2CS: 1NC: 1.5MIL-53(Fe).
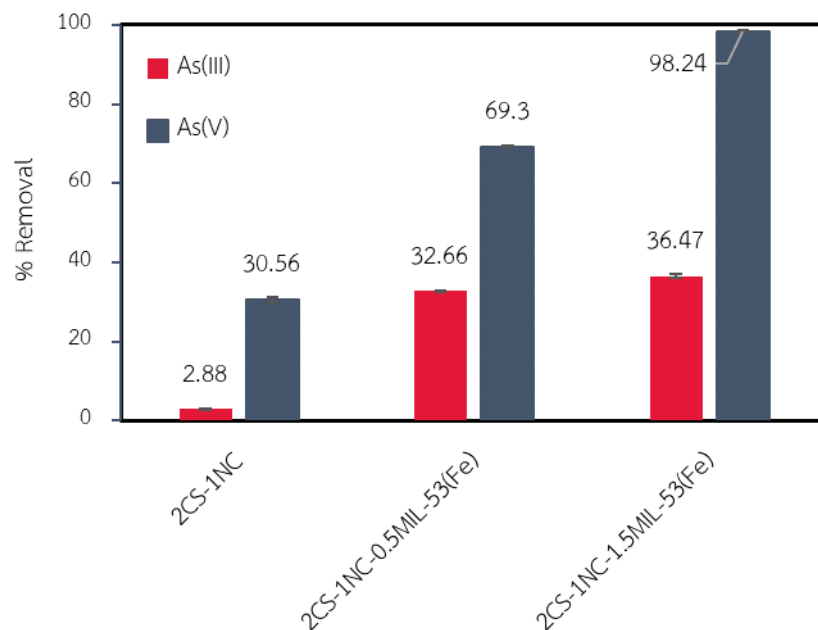
Figure 4.13 Efficiency of arsenic removal by 2CS-1NC, 2CS-1NC-0.5MIL-53(Fe), and 2CS-1NC-1.5MIL-53(Fe) composite (40 mg/L for As(III) and As(V), pH 5, 12 h).

4.4.2 Characterization

Surface area analysis

The specific surface area of CS-NC-MIL-53(Fe) composite was determined by nitrogen adsorption. The result indicated that the surface area of CS-NC-MIL-53(Fe) increased from 5.96 m^2 g^{-1} of CS-NC composite to 8.70 m^2 g^{-1}, implying that the MIL-53(Fe) crystals had an important role for enhancing the specific surface area of composite material.

Scanning electron microscopy (SEM)

The morphology of CS-NC-MIL-53(Fe) composite material was measured by SEM. The surface and cross-sectional morphology of the composite are presented in

Figure 4.14. A highly porous structure with different pore sizes was observed. The pores were filled with NC particles and the crystals of MIL-53(Fe).
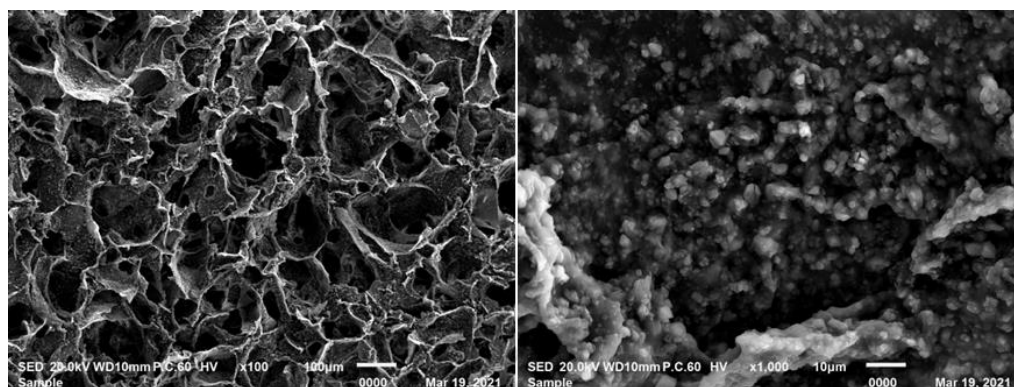
Figure 4.14 The cross-sectional SEM images of CS-NC-MIL-53(Fe).

Energy dispersive X-ray spectroscopy (EDX) and elemental mapping analysis

The elemental mapping was used to observe the distribution of Fe, O, and C on the CS-NC-MIL-53(Fe) surface. The results shown in Figure 4.15 indicated that MIL-53(Fe) particles were dispersed homogeneously on the surface of the composite material as confirmed by the distribution of Fe. Homogeneous distribution of C and O could be observed throughout the surface of the composite. The EDX spectrum of CS-NC-MIL-53(Fe) also revealed the presence of Fe, O, and C, corresponding to elemental mapping results (Table 4.9). Carbon and oxygen were found in large content due to the CS and NC component in the composite.

Table 4.9 Elemental composition of CS-NC-MIL-53(Fe) porous material

Element	Composition (%)
Carbon (C)	48.33
Oxygen (O)	33.99
Iron (Fe)	17.68
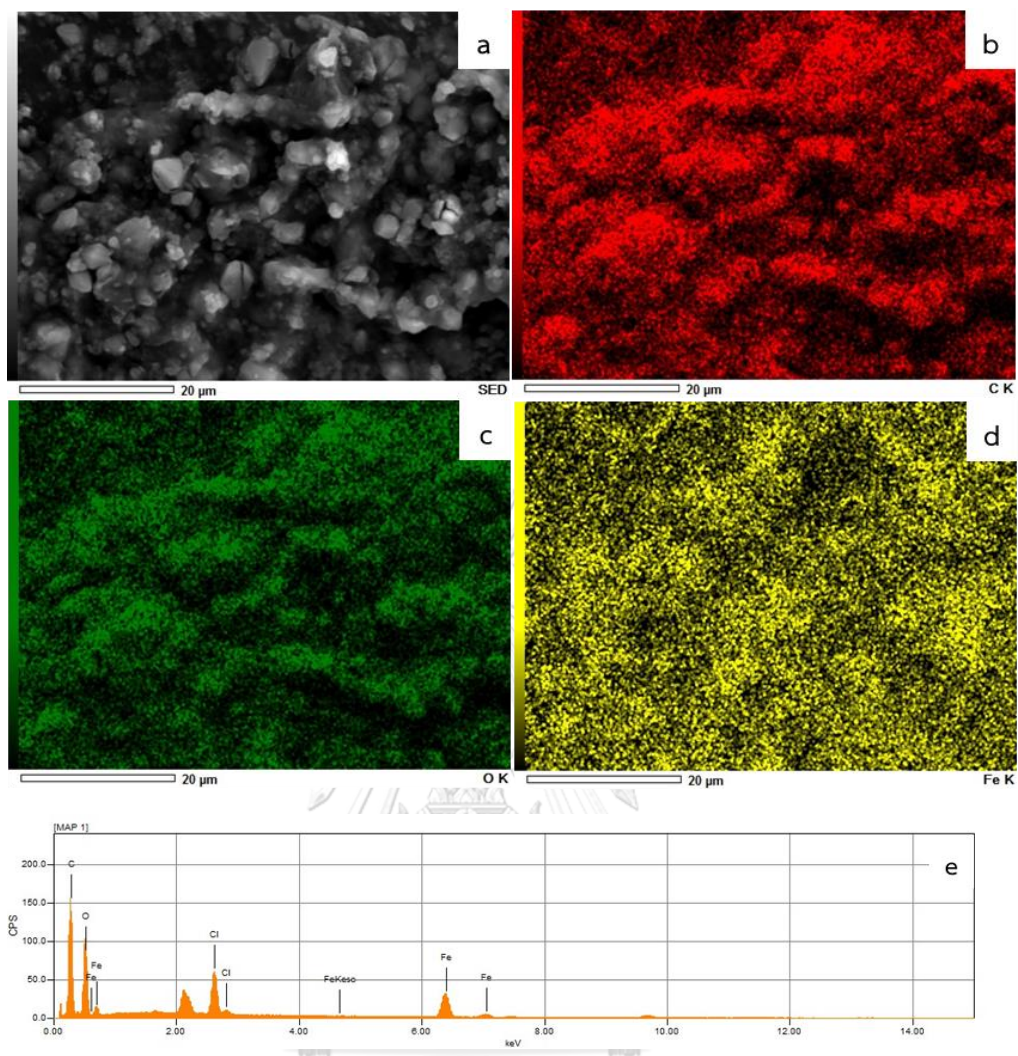
Figure 4.15 (a) SEM image, elemental mapping of (b) C, (c) O, and (d) Fe, and
(e) corresponding EDX of CS-NC-MIL-53(Fe).

The results from the surface area, SEM, EDX, and elemental mapping analysis confirmed the successful modification of CS-NC composite material with MIL-53(Fe). The CS-NC-MIL-53(Fe) was further used in the adsorption of As(III) and As(V) in aqueous solutions.

4.5 Adsorption study

By designing this adsorptive material, the expected adsorption mechanisms were the interaction between anionic As(III) and As(V) species and protonated amine groups on CS chain via electrostatic attraction [20-22]. For the MIL-53(Fe) in the adsorbent, the Fe^{3+} cation of MIL-53 could form complex with arsenic through the Lewis acid – base interaction [38].

4.5.1 Effect of initial pH of the arsenic solution

As shown in Figure 4.16, the effect of initial pH in the range of 3 to 11 on the removal of As(III) and As(V) by CS-NC-MIL-53(Fe) adsorbent were demonstrated. The results show that the pH in this range did not affect the efficiency in As(V) removal. As(V) species in solution of this pH range appeared in its anionic forms as $H_2AsO_4^-$, $HAsO_4^{2-}$, and AsO_4^{3-}. Under acidic condition, these species could be removed from solution via electrostatic interaction with the protonated amine groups ($-NH_3^+$) of CS component. In addition, Fe^{3+} in the MIL-53 frameworks (Lewis acid) would strongly interact with these anionic ligands of As(V) (Lewis base), donating a pair of electrons to the Fe^{3+}. On the other hand, at high pH, the amine groups of chitosan were in its neutral form ($pK_a = 6.5$) [62] and would interact with anionic arsenic species through Lewis acid-base interaction. It was observed that the final pH of all the solution was in a range of 3.5-6.3. As the CS-NC-MIL-53(Fe) adsorbent was prepared in acidic condition, it was likely that the materials contained acid that was released to the solution causing the pH of solution gradually reverse to acid. During the change of solution pH, various interactions described previously probably occurred, leading to the adsorption of As(V) onto the material. Therefore, CS-NC-MIL-53(Fe) sorbent could be used in a wide pH range for As(V) adsorption.

Meanwhile, the As(III) removal increased with increasing the initial pH of the solution. In solution having pH below 7, As(III) existing as H_3AsO_3 would not interact

with protonated amine of CS in the sorbent, and only coordination with Fe^{3+} in the MIL-53 frameworks attributed to As(III) removal. In addition, when raised the solution pH higher than 7, the amine group existed in its neutral form and could also interact with the As(III) in form of $H_2AsO_3^-$ and $HAsO_3^{2-}$ through Lewis acid-base interaction. Hence, the removal of As(III) removal efficiency increased in raising the solution pH. Thus, the removal of As(III) by this adsorbent should be performed in basic condition. The CS-NC-MIL-53(Fe) exhibited the highest removal efficiency at pH 11 and pH 5-9 for As(III) and As(V), respectively. The further experiment for As(III) and As(V) adsorption was performed in solution with initial pH of 9.
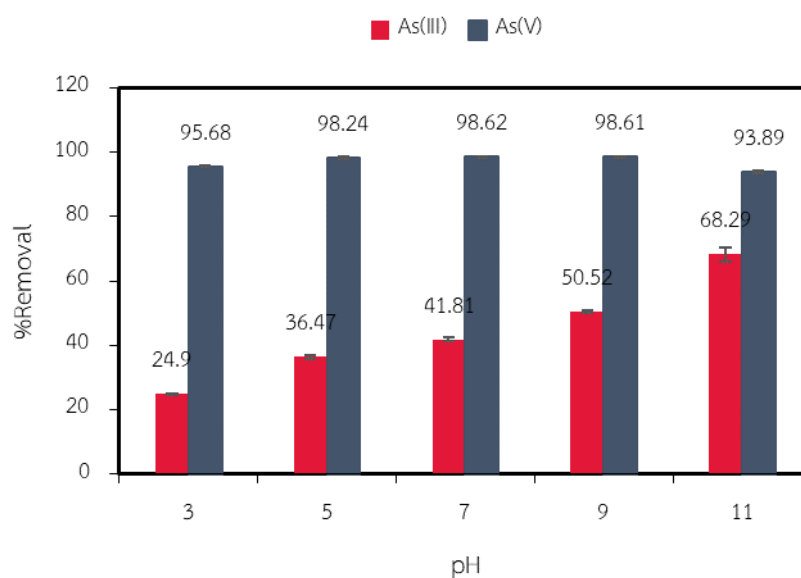
Figure 4.16 Effect of pH on the removal of the As(III) and As(V) by CS-NC-MIL-53(Fe).

4.5.2 Effect of contact time

In this experiment, the effect of contact time on the arsenic adsorbed on CS-NC-MIL-53(Fe) composite at 25°C was studied in the range of 0.5 to 15 h (Figure 4.17). The results indicated that the adsorption of both As(III) and As(V) occurred slowly and reached the equilibrium after 6 h. The low adsorption rate could be

explained by the dense structure of adsorbent as the MIL-53(Fe) distributed inside the pores of the composite material. The mass transfer of arsenic ions from bulk solution to the pores inside the material for further adsorption was likely to be slow, compared to highly porous materials.
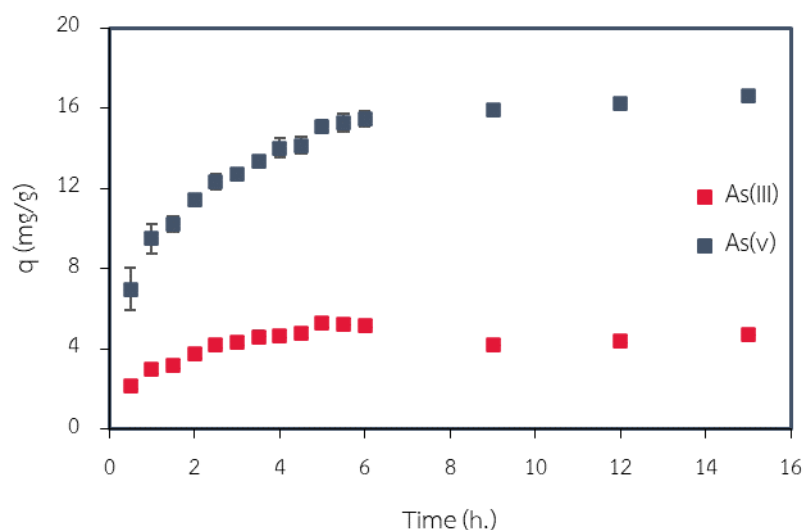
Figure 4.17 Effect of contact time on the adsorption of As(III) and As(V) by CS-NC-MIL-53(Fe) (initial concentration of 40 mg/L for As(III) and As(V)).

4.5.3 Adsorption kinetics

To investigate the adsorption kinetics for further understanding the adsorption behavior, the adsorption data of As(III) and As(V) from previous experiment (4.5.2) were fitted to pseudo-first-order and pseudo-second-order kinetic models. The equations of these two models are expressed in equation 4.1 [45] and 4.2 [44], respectively. The variable q_e and q_t is the amount of arsenic adsorbed at equilibrium (mg/g) and at time t (min), respectively. k_1 and k_2 is the rate constant of the pseudo-first order adsorption (min^{-1}) and the pseudo-second order adsorption (g/mg.min), respectively. The k_1 and k_2 could be calculated from the slope and the intercept of the linear plots, respectively.

$$\log(q_e - q_t) = \log q_e - \frac{k_1}{2.303}t \tag{4.1}$$

$$\frac{t}{q_t} = \frac{1}{k_2 q_e^2} + \frac{t}{q_e} \tag{4.2}$$

The results of As(III) and As(V) adsorption were fitted to the linear form following the two kinetic models as presented in Figure 4.18 - 4.19 and Table 4.10. The adsorption kinetics of As(III) and As(V) could not be explained by pseudo-first order model as the plot did not give linear relationship. In addition, the calculated adsorption capacity at equilibrium ($q_{e,cal}$) of both As(III) and As(V) from the linear plot did not correspond with the adsorption capacity at equilibrium observed in the experiment ($q_{e,exp}$). On the other hand, the adsorption kinetics of As(III) and As(V) followed the pseudo-second order kinetic model as the correlation coefficients (R^2) of linear regression were 0.984 and 0.999, respectively. The $q_{e,cal}$ were also close to $q_{e,exp}$, demonstrating that the kinetic model fitted well to the experimental data.

As the adsorption kinetics of As(III) and As(V) on the CS-NC-MIL-53(Fe) composite followed the pseudo-second order model, it suggested, as the hypothesis of the model, that the adsorption may occur through chemisorption. In this case, the expected mechanism was the complex formation between oxyanions of arsenic and adsorptive sites (Fe^{3+}) on the adsorbent.
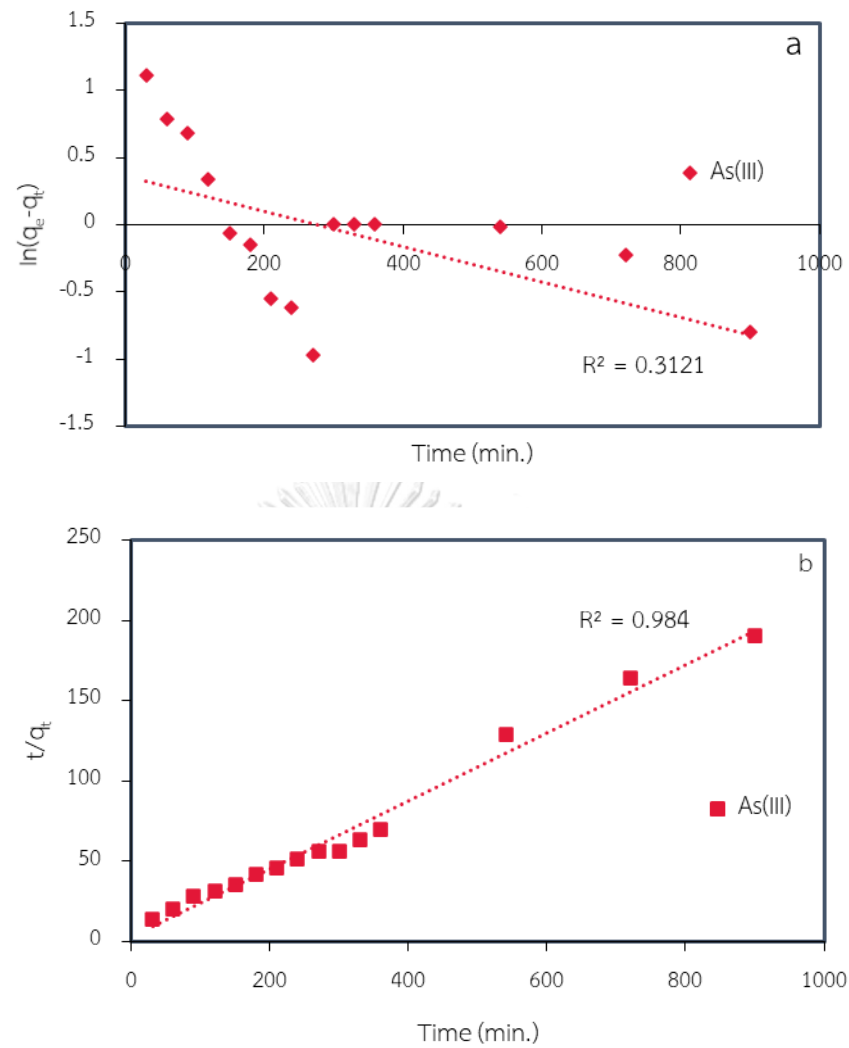
Figure 4.18 Linear plot of (a) pseudo-first order and (b) pseudo-second order kinetic model for the adsorption of As(III) on CS-NC-MIL-53(Fe) composite adsorbent.
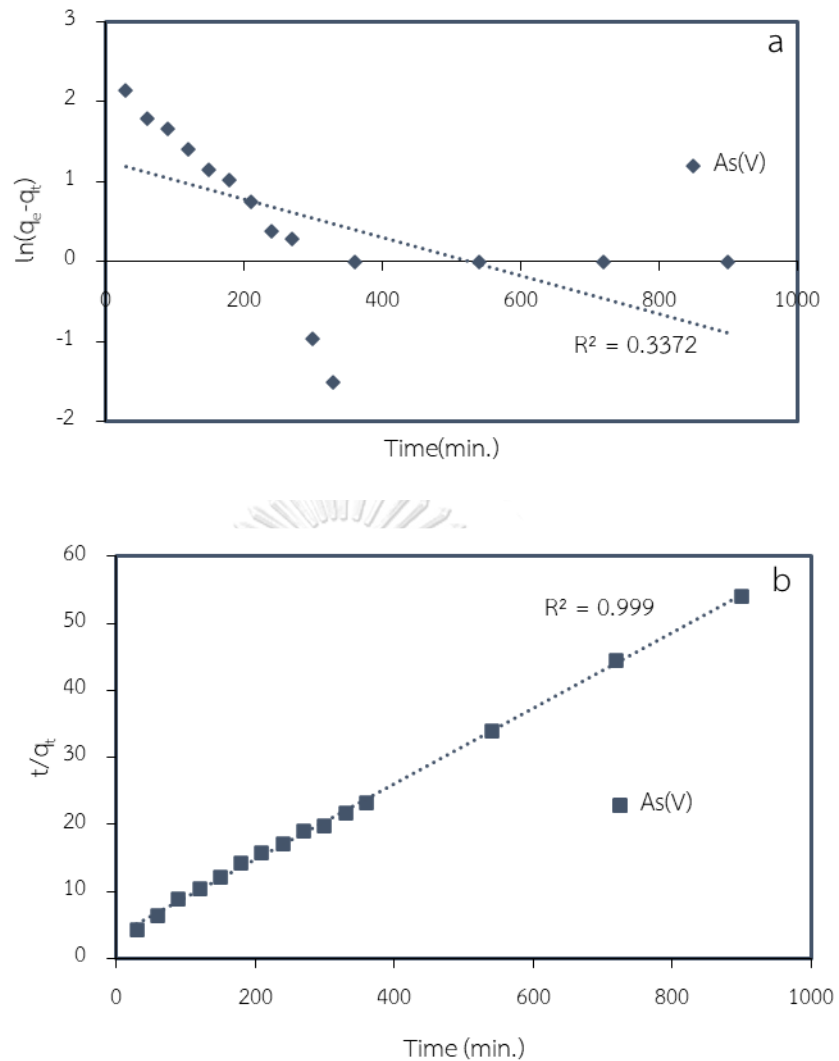
Figure 4.19 Linear plot of (a) pseudo-first order and (b) pseudo-second order kinetic model for the adsorption of As(V) on CS-NC-MIL-53(Fe) composite adsorbent.

Table 4.10 The kinetics parameter and constants for the adsorption of As(III) and As(V) on CS-NC-MIL-53(Fe) composite

Metal	$q_{e,exp}$ (mg/g)	Pseudo-first order model				Pseudo-second order			
		Linear equation	$q_{e,cal}$ (mg/g)	$k_1 \times 10^{-4}$ (min^{-1})	R_1^2	Linear equation	$q_{e,cal}$ (mg/g)	$k_2 \times 10^{-3}$ (g/mg.min)	R_2^2
As(III)	5.18	y=-0.0013x + 0.3636	2.31	5.64	0.312	y=0.2115x + 3.0496	4.73	12.10	0.984
As(V)	15.48	y=-0.0024x + 1.2557	18.0	10.42	0.337	y=0.0565x + 3.3981	17.70	1.20	0.999

4.5.4 Adsorption isotherms

The adsorption behavior of As(III) and As(V) onto CS-NC-MIL-53(Fe) at equilibrium can be described by the adsorption isotherm studies. In this experiment, a piece of CS-NC-MIL-53(Fe) (40 mg) was used in the adsorption of As(III) and As(V) in solutions (20 mL) containing different concentrations of As(III) and As(V) from 5 to 50 mg/L and 20 to 175 mg/L, respectively, with the initial pH value of 9. The contact time was fixed at 12 h to ensure that the equilibrium was reached and the experiment was performed at 25°C. The experimental data of As(III) and As(V) adsorption at equilibrium were fitted with the Langmuir, Freundlich, Temkin, and Dubinin-Radushkevich (DR) isotherm models.

The Langmuir isotherm was used to describe a monolayer adsorption on the specific or homogeneous surface of adsorbent where each active site adsorbs only one molecule or ion. The Langmuir adsorption isotherm equation is shown in equation 4.3 [46];

$$\frac{C_e}{q_e} = \frac{1}{bq_m} + \frac{C_e}{q_m} \tag{4.3}$$

C_e is the equilibrium concentration of arsenic in aqueous solution (mg/L), q_e and q_m is the amount of arsenic adsorbed at equilibrium (mg/g) and maximum adsorption capacity of arsenic (mg/g), respectively. The constant b is Langmuir constant related to the affinity of binding sites (L/mg). From the equation 4.3, the

value of q_m and b are obtained from the slope and intercept of the linear equation obtained by plotting C_e/q_e against C_e.

The Freundlich isotherm model can be used to describe the adsorptions on active sites of various affinity or heterogeneous surface. In addition, the adsorption on the adsorbent may occur as multilayer or monolayer regime. The isotherm equation is expressed as follows [47].

$$\log q_e = \log K_F + \frac{1}{n} log C_e \qquad (4.4)$$

K_F is Freundlich constant related to adsorption capacity (mg/g) and n is Freundlich constant related to adsorption intensity. From equation 4.5, K_F and n can be determined from the linear plotting of $\log q_e$ versus $\log C_e$.

Temkin isotherm model is used to indirectly describe adsorbate interactions in the adsorption process that is related to the heat of adsorption. The linear equation of Temkin isotherm is expressed following equation 4.5 [47, 50].

$$q_e = \frac{RT}{b} \ln A + \frac{RT}{b} ln C_e \qquad (4.5)$$

R is gas constant (8.31 J/mol K) and T is absolute temperature (K). The constant b and A is the constant related to the heat of sorption (J/mol) and Temkin isotherm constant (L/g), respectively. The value of A and b can be determined from the linear plot of q_e versus $\ln C_e$.

Dubinin-Radushkevich (DR) isotherm is applied to express adsorption mechanism with energy distribution on heterogeneous surfaces that is related to the adsorption energy. The equation of Dubinin-Radushkevich isotherm is expressed as followed [47].

$$ln q_e = ln q_m - \beta \varepsilon^2 \qquad (4.6)$$

$$\varepsilon = RT ln(1 + \frac{1}{C_e}) \qquad (4.7)$$

$$E = \frac{1}{\sqrt{2\beta}} \qquad (4.8)$$

β is DR constant related the adsorption free energy (E) (mol^2/J^2), while ε is Polanyi potential. From the equation 4.6, a linear equation was obtained by plotting $ln\,q_e$ against ε^2, where ε^2 is based on temperature, gas constant, and equilibrium concentration. The value of q_m and β were obtained from the intercept and slope of the linear equation.

As shown in Figure 4.20, the results demonstrated that the adsorption of both As(III) and As(V) on CS-NC-MIL-53(Fe) shown as the amount adsorbed at equilibrium (q_e) increased with increasing the initial concentration and gradually reached relatively constant values. These results indicated the saturation of arsenic on the solid surface, with no further adsorption despite increasing solution concentration. The experimental data were used in the linear plots following the linear form of Langmuir, Freundlich, Temkin, and Dubinin and Radushkevich (DR) models (Figure 4.21 – 4.24). The parameters of these isotherms for As(III) and As(V) adsorption calculated from curve fitting are listed in Table 4.11.
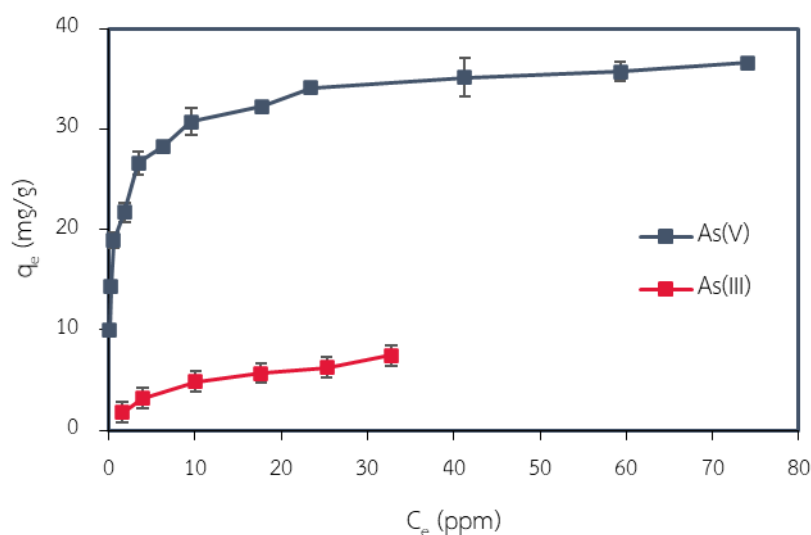
Figure 4.20 Adsorption isotherms of As(III) and As(V) on CS-NC-MIL-53(Fe).
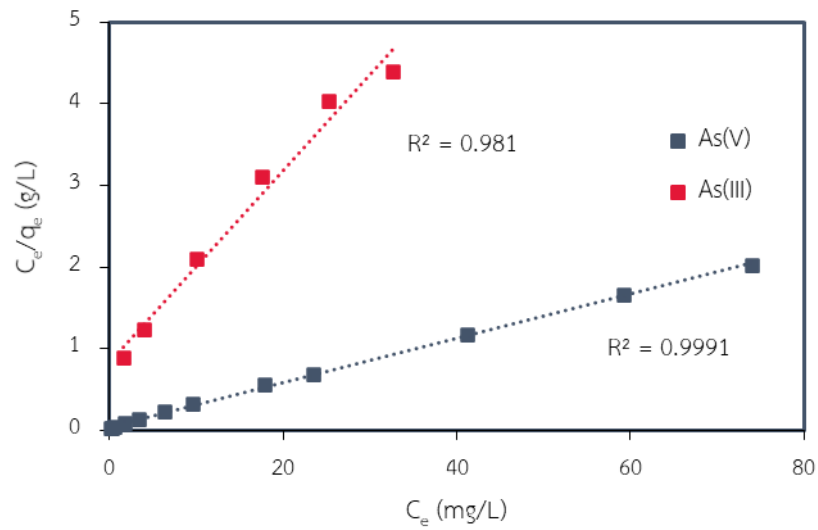
Figure 4.21 Langmuir isotherm plot of As(III) and As(V) adsorption on
CS-NC-MIL-53(Fe).
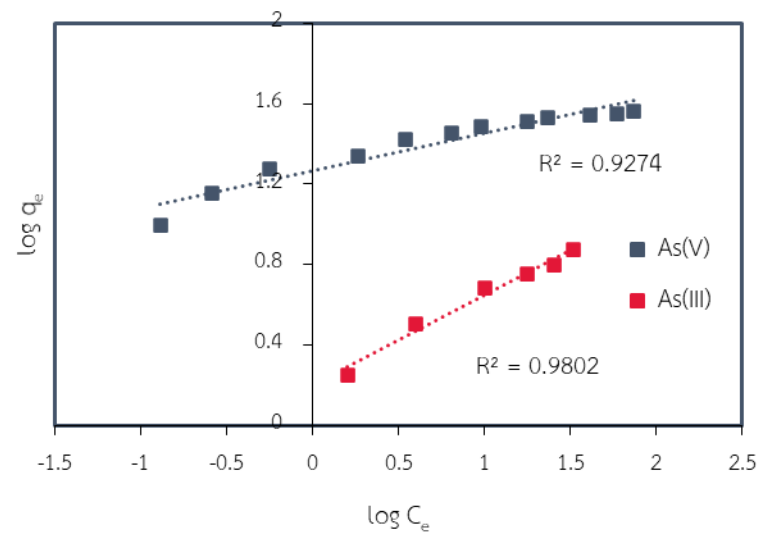
Figure 4.22 Freundlich isotherm plot of As(III) and As(V) adsorption on
CS-NC-MIL-53(Fe).
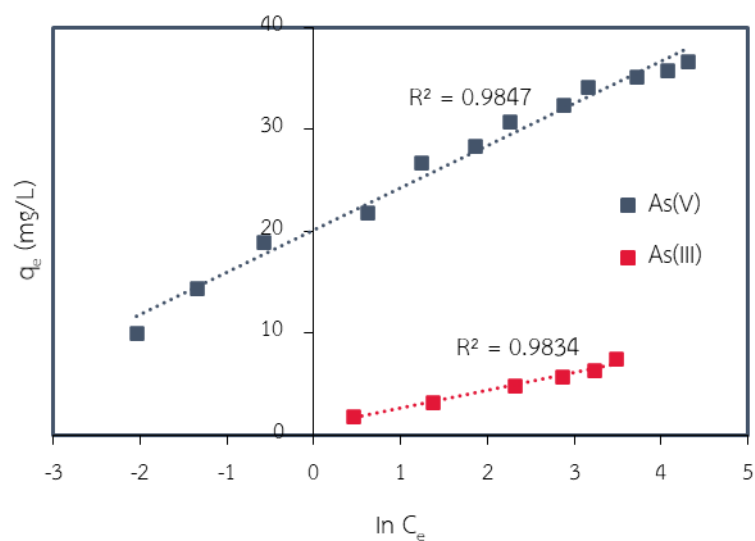
Figure 4.23 Temkin isotherms plot of As(III) and As(V) adsorption on
CS-NC-MIL-53(Fe).
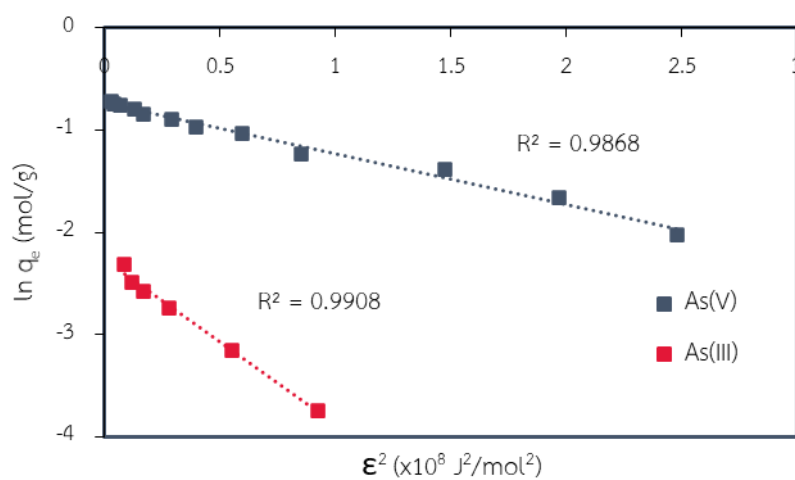
Figure 4.24 Dubinin-Radushkevich isotherm plot of As(III) and As(V) adsorption
on CS-NC-MIL-53(Fe).

Table 4.11 Parameters of the applied adsorption isotherm models

| Isotherm models	As(III)	As(V)
$q_{e,exp}$ (mg/g)	**7.46**	**36.66**
Langmuir isotherm		
Linear equation	y=0.1172x + 0.8398	y=0.0272x + 0.0353
q_m (mg/g)	8.53	36.76
b (L/mg)	0.14	0.77
R_L	0.125 – 0.588	0.007 – 0.061
R^2	0.981	0.999
Freundlich isotherm		
Linear equation	y=0.448x + 0.1986	y=0.1858x + 1.2677
K_F (mg/g)	1.58	18.52
n	2.23	5.38
R^2	0.980	0.926
Temkin isotherm		
Linear equation	y=1.7661x + 0.8285	y=4.1472x + 20.091
A (L/g)	1.599	127.7
b (kJ/mol)	1.403	0.598
R^2	0.983	0.985
Dubinin-Radushkevich isotherm		
Linear equation	y=-1.6206x – 2.26	y=-0.4932x – 0.7363
β (mol^2/kJ^2)	1.6206	0.4932
E (kJ/mol)	0.56	1.01
R^2	0.991	0.987

The results as shown in Table 4.11, indicated that the adsorption of As(III) and As(V) on CS-NC-MIL-53(Fe) could be described by the Langmuir model ($R^2 > 0.98$). The obtained calculated maximum adsorption capacities (q_m) were also close to the values observed in the experiments ($q_{e,exp}$), indicating the good fitting of the model to the experimental data. Therefore, the adsorption of As(III) and As(V) on CS-NC-MIL-53(Fe), as in the hypothesis of Langmuir isotherm, occurred as monolayer adsorption. Moreover, the calculated R_L values were in the range of $0 < R_L < 1$,

indicating that the adsorption of As(III) and As(V) on the composite sorbent were favorable [46, 49]. In the Freundlich model plot, the correlation coefficients (R^2) obtained were high for both As(III) and As(V), which may be explained by the adsorption of arsenic on heterogeneous active sites which were amine groups and MIL-53(Fe) in the composite material. However, considering the constants related to the adsorption capacity, the adsorption of As(III) and As(V) could be better described by Langmuir model.

According to the Temkin model, the heat (b) of As(III) and As(V) adsorption process was estimated to be 1.403 and 0.598 kJ/mol, respectively, indicating an endothermal adsorption processes. Moreover, the adsorption free energy (E) of As(III) and As(V) calculated from the DR model was 0.56 and 1.01 kJ/mol, respectively. The E values fell in the range of the physical adsorption (E < 8 kJ/mol). It might be explained that mixed adsorption mechanisms (i.e. electrostatic interaction or physisorption and coordination or chemisorption) occurred on the composite, and therefore, the obtained E values were likely to be the average value of these mechanisms [51].

From all the results, it could be confirmed that the adsorption process occurred as a monolayer of arsenic species on the specific active sites on adsorbent and possibly took place through electrostatic interaction and coordination mechanism.

The performance and the adsorption capacity of CS-NC-MIL-53(Fe) for As(III) and As(V) adsorption were compared to other materials previously reported as shown in Table 4.12. The prepared CS-NC-MIL-53(Fe) adsorbent in this work has satisfactory adsorption capacity for As(III) and As(V) with shorter contact time. The material can be used in a wide pH range for As(V) removal, while it can be used to adsorb As(III) in basic solution to get the best performance.

Table 4.12 Comparison of the As(III) and As(V) adsorption capacity of different adsorbents

Adsorbent	Arsenic species	Adsorption capacity (mg/g)	pH	Time (h)	Reference
ZrO$_2$-immobilized alginate beads	As(III)	32.3	5	240	[46]
	As(V)	28.5			
MIL-100(Fe) modified bacterial cellulose nanocomposite	As(III)	4.8	-	72	[63]
UiO-66/PAN nanofibers	As(III)	32.90	7	24	[64]
	As(V)	42.17			
PG/MOF composite nanofibers	As(V)	180	5	24	[65]
Chitosan-nanocellulose composite modified with MIL-53(Fe) (CS-NC-MIL-53(Fe))	As(III)	8.53	9	12	**This work**
	As(V)	36.76	9		

4.5.5 Effect of potential interfering ions

Typically, As(III) or As(V) coexists with other ions in natural water and wastewater that may competitively adsorb on CS-NC-MIL-53(Fe) adsorbent. Considering the properties of CS-NC-MIL-53(Fe) adsorbent, the amine groups of chitosan could be protonated under acidic conditions and acted as active sites for anionic species such as sulfate and phosphate. On the other hand, under basic conditions, the amine groups are present in a neutral form that can form complex with other heavy metal ions (transition metal ions) via Lewis acid-base interaction. Meanwhile, the Fe^{3+} cations (Lewis acid) in MIL-53(Fe) can interact with ligands (Lewis

base) such as sulfate and phosphate. Therefore, the influence of these interfering ions were investigated.

In this experiment, the effect of anions (SO_4^{2-} and PO_4^{3-}), cations (Na^+ and Mg^{2+}), and heavy metal ions (CrO_4^{2-}, Mn^{2+}, Fe^{3+}, Ni^{2+}, Cu^{2+}, Zn^{2+}, Cd^{2+}, and Pb^{2+}) were examined using the concentration equal to 0.4 mM As(III) and 0.8 mM As(V) and 10 times higher in binary mixtures system. The solution initial pH was adjusted to 9 and contact time was fixed to 12 h. By adjusting to pH 9, most heavy metal ions (Mn^{2+}, Fe^{3+}, Ni^{2+}, Cu^{2+}, Zn^{2+}, Cd^{2+}, and Pb^{2+}) precipitated from solution, and hence, only the binary mixtures with CrO_4^{2-} were used in this study. The results are shown in Table 4.13.

Table 4.13 Effect of interfering ions on the adsorption of As(III) and As(V) by CS-NC-MIL-53(Fe)

Interfering ions	As(III)*		As(V)*	
	Concentration of salt (mM)	Adsorption capacity (mg/g)	Concentration of salt (mM)	Adsorption capacity (mg/g)
Blank	-	4.30 ± 0.15	-	27.61 ± 0.70
Na_2SO_4	0.4	4.27 ± 0.15	0.8	23.11 ± 1.07
	4.0	5.29 ± 0.36	8.0	22.37 ± 0.14
Na_2HPO_4	0.4	3.00 ± 0.08	0.8	21.68 ± 0.34
	4.0	2.39 ± 0.07	8.0	10.04 ± 0.12
$MgSO_4$	0.4	4.07 ± 0.13	0.8	23.39 ± 0.02
	4.0	4.94 ± 0.74	8.0	22.80 ± 1.66
K_2CrO_4	0.4	11.09 ± 0.27	0.8	24.17 ± 0.43
	4.0	-**	8.0	-**

*The concentration of As(III) and As(V) were 0.4 and 0.8 mM, respectively.

**Not performed

For the effect of anions, the presence of SO_4^{2-} had slight effects on As(III) and As(V) adsorption in most cases, as the adsorbed amount of As(III) and As(V) slightly decreased. On the other hand, the adsorption capacity for As(III) and As(V) was remarkably reduced by the presence of PO_4^{3-}, especially at the high concentration. These anions could compete with arsenite and arsenate for the adsorption through both electrostatic attraction and complex formation with Fe^{3+}. However, the materials still showed good affinity towards As(III) and As(V), despite the presence of these interfering anions 10 times higher. Interestingly, the presence of SO_4^{2-} at high concentration enhanced the adsorption of As(III).

In the case of Na_2SO_4 and $MgSO_4$ salts in arsenic solutions, there was no significant difference in adsorption capacity of both As(III) and As(V) when the type of salts changed at 95% confidence level. Hence, the type of cations did not show interfering effect and it agreed well with the adsorption mechanism.

For the effect of CrO_4^{2-}, it showed a slight effect on As(V) adsorption, likely through competitive interaction with both amine groups and Fe(III) centers. Surprisingly, it enhanced the adsorption of As(III) on the materials. The effect of high concentration CrO_4^{2-} was not investigated because it is a rare case to find this level of Cr(VI) in the water sources containing arsenic, either natural water or wastewater.

4.6 Application to real water sample

The CS-NC-MIL-53(Fe) composite was applied to remove arsenic in real water samples. In this work, wastewater samples from a petroleum refining industry (Thailand) were collected and used in the adsorption experiments. The first source of wastewater had a low concentration (4.09 mg/L) of total arsenic with basic pH (pH 9.2), while the second source had a high arsenic concentration (736.02 mg/L) with the pH of 6.8. Thus, the second source waste was diluted 20 times and adjusted

the pH to 9. The adsorption experiments were performed by using 1, 2, or 3 pieces of CS-NC-MIL-53(Fe) composite in 20 mL of samples with the contact time of 12 h.

As shown in Figure 4.25, a piece of adsorbent could remove 93.95% of arsenic in the first wastewater source to reduce the arsenic concentration to lower than 0.25 mg/L. For the second source, the removal efficiency increased from 51.52 to 68.78 % with increasing the amount of CS-NC-MIL-53(Fe) material. These results confirmed that the CS-NC-MIL-53(Fe) composite material can be applied to remove arsenic in the real water samples.
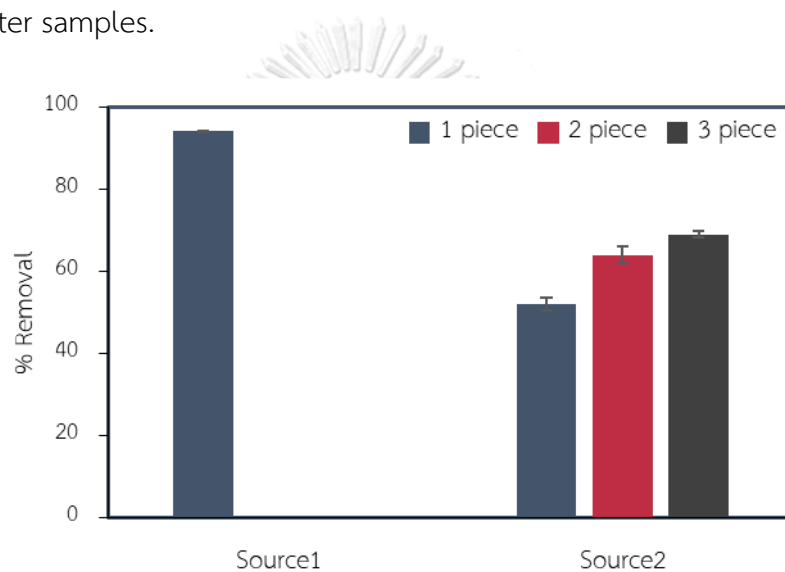
Figure 4.25 The removal of arsenic in wastewater sample by CS-NC-MIL-53(Fe) material (initial arsenic concentration of source1 and source2 was 4.09 and 32.17 mg/L, respectively).

CHAPTER 5

CONCLUSIONS

Nanocellulose particles and MIL-53(Fe) metal-organic frameworks were synthesized and used to prepare a composite material. The nanocellulose exhibited the spherical shape with an average size in the range of 135.8 – 177.8 nm, while the MIL-53(Fe) showed the octahedron crystalline structure. A new CS-NC-MIL-53(Fe) composite sponge was successfully fabricated by mixing chitosan, nanocellulose, and MIL-53(Fe), crosslinking with glutaraldehyde and N, N'-methylenebisacrylamide, and freeze-drying. The MIL-53(Fe) was added to enhance the adsorption efficiency. The morphology of the composite displayed a highly porous structure with a uniform distribution of nanocellulose and MIL-53(Fe) inside the pores. The composite sponge had good mechanical property due to the reinforcement by nanocellulose and therefore, it showed a good stability in water. The effect of NC and MIL-53(Fe) content were investigated, and the conditions for preparing the composite sponge were optimized. The most suitable weight ratio for the composite preparation was 2CS: 1NC: 1.5MIL-53(Fe).

In the adsorption study, the CS-NC-MIL-53(Fe) composite was used to remove As(III) and As(V) in aqueous solutions. The effect of initial pH of arsenic solution, contact time, initial concentration, and potential interfering ions were investigated. The adsorption behavior and suitable conditions for removing As(III) and As(V) in solution by CS-NC-MIL-53(Fe) composite are listed in Table 5.1. The adsorption occurred as monolayer on the surface of CS-NC-MIL-53(Fe) via the electrostatic interaction with protonated amine groups on chitosan and coordination with Fe(III) in MIL-53(Fe). It was observed that the capacity of the material for As(V) adsorption was greater than that of As(III). However, the adsorption of arsenic could be interfered by the presence of SO_4^{2-} and PO_4^{3-} in the solution. These anions could competitively

interact with amine groups of chitosan through electrostatic interaction and their chemical structure are also similar to arsenite and arsenate anion.

The application of the material to treat wastewater from a petroleum refining industry was demonstrated. The results showed that the CS-NC-MIL-53(Fe) composite could remove arsenic in a real wastewater matrix with a good efficiency.

Table 5.1 The adsorption behavior of As(III) and As(V) on the CS-NC-MIL-53(Fe)

Parameter	Adsorption behavior	
	As(III)	As(V)
Initial pH of solution	9-11	3-11
Contact time	6 h	6 h
Kinetic model	Pseudo-second order	Pseudo-second order
Adsorption isotherm	Langmuir isotherm	Langmuir isotherm
Maximum adsorption capacity	8.53 mg/g	36.76 mg/g
Adsorption heat (from Temkin isotherm)	1.403 kJ/mol	0.598 kJ/mol
Interfering ions	SO_4^{2-} (weak) PO_4^{3-} (strong)	SO_4^{2-} (weak) PO_4^{3-} (strong)

Suggestion for future work

- The reusability of the materials as well as the stability in a long run treatment should be investigated.
- Because the CS-NC-MIL-53(Fe) has amine groups ($-NH_2$), the adsorbent may be applied to remove other heavy metal ions in other types of wastewaters to expand their application.
- Due to the presence of electron acceptor site as iron in the MIL-53 on the adsorbent, the composite may be applied for phosphate removal from water.

REFERENCES

1. Boyd, R.S., *Heavy metal pollutants and chemical ecology: exploring new frontiers.* Journal of chemical ecology, 2010. **36**(1): p. 46-58.

2. Pan, K. and Wang, W.X., *Trace metal contamination in estuarine and coastal environments in China.* Science of the Total Environment, 2012. **421-422**: p. 3-16.

3. Hao, J., et al., *SERS detection of arsenic in water: A review.* Journal of Environmental Sciences (China), 2015. **36**: p. 152-62.

4. Gomez-Caminero, A., et al., *Arsenic and arsenic compounds.* 2001, World Health Organization: Geneva.

5. Chowdhury, S.R. and Yanful, E.K., *Arsenic removal from aqueous solutions by adsorption on magnetite nanoparticles.* Water and Environment Journal, 2011. **25**(3): p. 429-437.

6. *Locating and estimating air emissions from sources of arsenic and arsenic compounds. Final report.* 1998: United States.

7. Fowler, B.A., et al., *CHAPTER 19 - Arsenic,* in *Handbook on the Toxicology of Metals (Third Edition),* G.F. Nordberg, et al., Editors. 2007, Academic Press: Burlington. p. 367-406.

8. Yeo, K.F.H., et al., *Arsenic Removal from Contaminated Water Using Natural Adsorbents: A Review.* Coatings, 2021. **11**(11).

9. *Environment quality standard in Thailand.* 2018, Pollution Control Department of Thailand (PCD): Thailand. p. 1-45.

10. Maity, S., et al., *A study on arsenic adsorption on polymetallic sea nodule in aqueous medium.* Water Research, 2005. **39**(12): p. 2579-2590.

11. Samuel, M.S., et al., *Nanomaterials as adsorbents for As(III) and As(V) removal from water: A review.* Journal of Hazardous Materials, 2022. **424**: p. 127572.

12. Nicomel, N.R., et al., *Technologies for Arsenic Removal from Water: Current Status and Future Perspectives.* International Journal of Environmental Research and Public Health, 2016. **13**(1): p. 62.

13. Pattanayak, J., et al., *A parametric evaluation of the removal of As(V) and As(III) by

carbon-based adsorbents. Carbon, 2000. **38**(4): p. 589-596.

14. Singh, T.S. and Pant, K.K., *Equilibrium, kinetics and thermodynamic studies for adsorption of As(III) on activated alumina.* Separation and Purification Technology, 2004. **36**(2): p. 139-147.

15. Zeng, L., *A method for preparing silica-containing iron(III) oxide adsorbents for arsenic removal.* Water Research, 2003. **37**(18): p. 4351-4358.

16. Yu, X., et al., *Synthesis and characterization of multi-amino-functionalized cellulose for arsenic adsorption.* Carbohydrate Polymers, 2013. **92**(1): p. 380-387.

17. Muxika, A., et al., *Chitosan as a bioactive polymer: Processing, properties and applications.* International Journal of Biological Macromolecules, 2017. **105**: p. 1358-1368.

18. Dragan, E.S. and Dinu, M.V., *Advances in porous chitosan-based composite hydrogels: Synthesis and applications.* Reactive and Functional Polymers, 2020. **146**: p. 104372.

19. Thakur, V.K. and Thakur, M.K., *Recent Advances in Graft Copolymerization and Applications of Chitosan: A Review.* ACS Sustainable Chemistry & Engineering, 2014. **2**(12): p. 2637-2652.

20. Gérente, C., et al., *Removal of arsenic(V) onto chitosan: From sorption mechanism explanation to dynamic water treatment process.* Chemical Engineering Journal, 2010. **158**(3): p. 593-598.

21. Kwok, K.C.M., et al., *Adsorption/desorption of arsenite and arsenate on chitosan and nanochitosan.* Environmental Science and Pollution Research, 2018. **25**(15): p. 14734-14742.

22. Kwok, K.C.M., et al., *Mechanism of arsenic removal using chitosan and nanochitosan.* Journal of Colloid and Interface Science, 2014. **416**: p. 1-10.

23. Sokker, H.H., et al., *Adsorption of crude oil from aqueous solution by hydrogel of chitosan based polyacrylamide prepared by radiation induced graft polymerization.* Journal of Hazardous Materials, 2011. **190**(1): p. 359-365.

24. Pakdel, P.M. and Peighambardoust, S.J., *Review on recent progress in chitosan-based hydrogels for wastewater treatment application.* Carbohydrate Polymers, 2018. **201**: p. 264-279.

25. Zhang, H., et al., *A robust salt-tolerant superoleophobic chitosan/nanofibrillated cellulose aerogel for highly efficient oil/water separation.* Carbohydrate Polymers, 2018. **200**: p. 611-615.

26. H.P.S, A.K., et al., *A review on chitosan-cellulose blends and nanocellulose reinforced chitosan biocomposites: Properties and their applications.* Carbohydrate Polymers, 2016. **150**: p. 216-226.

27. Geng, CZ., et al., *Mechanically reinforced chitosan/cellulose nanocrystals composites with good transparency and biocompatibility.* Chinese Journal of Polymer Science, 2015. **33**(1): p. 61-69.

28. Zhang, D., et al., *A three-dimensional macroporous network structured chitosan/cellulose biocomposite sponge for rapid and selective removal of mercury(II) ions from aqueous solution.* Chemical Engineering Journal, 2019. **363**: p. 192-202.

29. Bian, Y., Xiong, N. and Zhu, G., *Technology for the Remediation of Water Pollution: A Review on the Fabrication of Metal Organic Frameworks.* Processes, 2018. **6**(8): p. 122.

30. Gao, Q., Xu, J. and Bu, XH., *Recent advances about metal–organic frameworks in the removal of pollutants from wastewater.* Coordination Chemistry Reviews, 2019. **378**: p. 17-31.

31. Du, JJ., et al., *New photocatalysts based on MIL-53 metal–organic frameworks for the decolorization of methylene blue dye.* Journal of Hazardous Materials, 2011. **190**(1): p. 945-951.

32. Yu, J., et al., *Functionalized MIL-53(Fe) as efficient adsorbents for removal of tetracycline antibiotics from aqueous solution.* Microporous and Mesoporous Materials, 2019. **290**: p. 109642.

33. Charpentier, T.V.J., et al., *Preparation of Magnetic Carboxymethylchitosan Nanoparticles for Adsorption of Heavy Metal Ions.* ACS Omega, 2016. **1**(1): p. 77-83.

34. Guleria, A., et al., *Removal of inorganic toxic contaminants from wastewater using sustainable biomass: A review.* Science of The Total Environment, 2022. **823**: p. 153689.

35. Mikušová, V. and Mikuš, P., *Advances in Chitosan-Based Nanoparticles for Drug*

Delivery. International Journal of Molecular Sciences, 2021. **22**(17): p. 9652.

36. Salih, S.S., et al., *Competitive adsorption of As(III) and As(V) onto chitosan/diatomaceous earth adsorbent.* Journal of Environmental Chemical Engineering, 2019. **7**(5): p. 103407.

37. Su, F., et al., *Three-dimensional honeycomb-like structured zero-valent iron/chitosan composite foams for effective removal of inorganic arsenic in water.* Journal of Colloid and Interface Science, 2016. **478**: p. 421-429.

38. Vu, T.A., et al., *Arsenic removal from aqueous solutions by adsorption using novel MIL-53(Fe) as a highly efficient adsorbent.* Royal Society of Chemistry Advances, 2015. **5**(7): p. 5261-5268.

39. Nguyen, D.T.C., et al., *Metal-Organic Framework MIL-53(Fe) as an Adsorbent for Ibuprofen Drug Removal from Aqueous Solutions: Response Surface Modeling and Optimization.* Journal of Chemistry, 2019. **2019**: p. 5602957.

40. Ghasemzadeh, M.A., Mirhosseini-Eshkevari, B. and Abdollahi-Basir, M.H., *MIL-53(Fe) Metal-Organic Frameworks (MOFs) as an Efficient and Reusable Catalyst for the One-Pot Four-Component Synthesis of Pyrano[2,3-c]-pyrazoles.* Applied Organometallic Chemistry, 2019. **33**(1): p. 1-8.

41. Erkey, C. and Türk, M., *Chapter 6 - Thermodynamics and kinetics of adsorption of metal complexes on surfaces from supercritical solutions*, in *Supercritical Fluid Science and Technology*, C. Erkey and M. Türk, Editors. 2021, Elsevier. p. 73-127.

42. *Physisorption vs. Chemisorption: The Two Adsorptions.* 2022, PSIBERGE Team: PSIBERGE.

43. Sahoo, T.R. and Prelot, B., *Chapter 7 - Adsorption processes for the removal of contaminants from wastewater: the perspective role of nanomaterials and nanotechnology*, in *Nanomaterials for the Detection and Removal of Wastewater Pollutants*, B. Bonelli, et al., Editors. 2020, Elsevier. p. 161-222.

44. Ho, Y.S. and McKay, G., *Pseudo-second order model for sorption processes.* Process Biochemistry, 1999. **34**(5): p. 451-465.

45. Akha, N.Z., Salehi, S. and Anbia, M., *Removal of arsenic by metal organic framework/chitosan/carbon nanocomposites: Modeling, optimization, and adsorption studies.* International Journal of Biological Macromolecules, 2022. **208**:

p. 794-808.

46. Kwon, OH., et al., *Adsorption of As(III), As(V) and Cu(II) on zirconium oxide immobilized alginate beads in aqueous phase.* Chemosphere, 2016. **160**: p. 126-133.

47. Ayawei, N., Ebelegi, A.N. and Wankasi, D., *Modelling and Interpretation of Adsorption Isotherms.* Journal of Chemistry, 2017. **2017**: p. 3039817.

48. Ma, J., et al., *Efficient Removal of Heavy Metal Ions with An EDTA Functionalized Chitosan/Polyacrylamide Double Network Hydrogel.* ACS Sustainable Chemistry & Engineering, 2017. **5**(1): p. 843-851.

49. Cho, DW., et al., *Adsorption of nitrate and Cr(VI) by cationic polymer-modified granular activated carbon.* Chemical Engineering Journal, 2011. **175**: p. 298-305.

50. Togue Kamga, F., *Modeling adsorption mechanism of paraquat onto Ayous (Triplochiton scleroxylon) wood sawdust.* Applied Water Science, 2018. **9**(1): p. 1-7.

51. Batool, F., et al., *Study of Isothermal, Kinetic, and Thermodynamic Parameters for Adsorption of Cadmium: An Overview of Linear and Nonlinear Approach and Error Analysis.* Bioinorganic Chemistry and Applications, 2018. **2018**: p. 3463724.

52. Shankar, S. and Rhim, JW., *Preparation of nanocellulose from micro-crystalline cellulose: The effect on the performance and properties of agar-based composite films.* Carbohydrate Polymers, 2016. **135**: p. 18-26.

53. Cai, J. and Zhang, L., *Rapid dissolution of cellulose in LiOH/urea and NaOH/urea aqueous solutions.* Macromolecular Bioscience, 2005. **5**(6): p. 539-48.

54. Xiong, B., et al., *Dissolution of cellulose in aqueous NaOH/urea solution: role of urea.* Cellulose, 2014. **21**(3): p. 1183-1192.

55. Csiszar, E., et al., *The role of the particle size reduction and morphological changes of solid substrate in the ultrasound-aided enzymatic hydrolysis of cellulose.* Ultrasonics Sonochemistry, 2021. **78**: p. 105711.

56. Lu, P. and Hsieh, YL., *Preparation and properties of cellulose nanocrystals: Rods, spheres, and network.* Carbohydrate Polymers, 2010. **82**(2): p. 329-336.

57. Adsul, M., et al., *Facile Approach for the Dispersion of Regenerated Cellulose in Aqueous System in the Form of Nanoparticles.* Biomacromolecules, 2012. **13**(9): p.

2890-2895.

58. Nguyen, V.H., et al., *Effective Photocatalytic Activity of Mixed Ni/Fe-Base Metal-Organic Framework under a Compact Fluorescent Daylight Lamp.* Catalysts, 2018. **8**(11): p. 487.

59. Llewellyn, P.L., et al., *Complex Adsorption of Short Linear Alkanes in the Flexible Metal-Organic-Framework MIL-53(Fe).* Journal of the American Chemical Society, 2009. **131**(36): p. 13002-13008.

60. Wang, X., et al., *Synthesis and characterization of a porous and hydrophobic cellulose-based composite for efficient and fast oil–water separation.* Carbohydrate Polymers, 2016. **140**: p. 188-194.

61. Kim, J., et al., *Preparation and characterization of a Bacterial cellulose/Chitosan composite for potential biomedical application.* Journal of Polymer Research, 2011. **18**(4): p. 739-744.

62. Mohammed, M.A., et al., *An Overview of Chitosan Nanoparticles and Its Application in Non-Parenteral Drug Delivery.* Pharmaceutics, 2017. **9**(4): p. 53.

63. Ashour, R.M., et al., *Green Synthesis of Metal-Organic Framework Bacterial Cellulose Nanocomposites for Separation Applications.* Polymers, 2020. **12**(5): p. 1104.

64. Guo, Q., et al., *Electrospun metal-organic frameworks hybrid nanofiber membrane for efficient removal of As(III) and As(V) from water.* Ecotoxicology and Environmental Safety, 2021. **228**: p. 112990.

65. Kong, L., et al., *One-step construction of hierarchical porous channels on electrospun MOF/polymer/graphene oxide composite nanofibers for effective arsenate removal from water.* Chemical Engineering Journal, 2022. **435**: p. 134830.

VITA

NAME	Yatika Paisart
DATE OF BIRTH	10 November 1995
PLACE OF BIRTH	Ubon Ratchathani
INSTITUTIONS ATTENDED	B.Sc., Chemistry, Science, Mahidol University, Bangkok, Thailand, July 2018.
HOME ADDRESS	107/62 Soi 24, Rama 6 Road, Thung Phaya Thai, Rat Thewi, Bangkok, Thailand, 10400

จุฬาลงกรณ์มหาวิทยาลัย
CHULALONGKORN UNIVERSITY